AGU PUBLICATIONS

JGR

Journal of Geophysical Research: Oceans

RESEARCH ARTICLE

10.1002/2015JC011405

Special Section:
Physical Processes Responsible for Material Transport in the Gulf of Mexico for Oil Spill Applications

Dispersion of a tracer in the deep Gulf of Mexico

James R. Ledwell[1], Ruoying He[2], Zuo Xue[3], Steven F. DiMarco[4], Laura J. Spencer[4], and Piers Chapman[4]

[1]Woods Hole Oceanographic Institution, Woods Hole, Massachusetts, USA, [2]Department of Marine, Earth, and Atmospheric Sciences, North Carolina State University, Raleigh, North Carolina, USA, [3]College of the Coast and Environment, Louisiana State University, Baton Rouge, Louisiana, USA, [4]Department of Oceanography, Texas A&M University, College Station, Texas, USA

Abstract A 25 km streak of CF_3SF_5 was released on an isopycnal surface approximately 1100 m deep, and 150 m above the bottom, along the continental slope of the northern Gulf of Mexico, to study stirring and mixing of a passive tracer. The location and depth of the release were near those of the deep hydrocarbon plume resulting from the 2010 Deepwater Horizon oil well rupture. The tracer was sampled between 5 and 12 days after release, and again 4 and 12 months after release. The tracer moved along the slope at first but gradually moved into the interior of the Gulf. Diapycnal spreading of the patch during the first 4 months was much faster than it was between 4 and 12 months, indicating that mixing was greatly enhanced over the slope. The rate of lateral homogenization of the tracer was much greater than observed in similar experiments in the open ocean, again possibly enhanced near the slope. Maximum concentrations found in the surveys had fallen by factors of 10^4, 10^7, and 10^8, at 1 week, 4 months, and 12 months, respectively, compared with those estimated for the initial tracer streak. A regional ocean model was used to simulate the tracer field and help interpret its dispersion and temporal evolution. Model-data comparisons show that the model simulation was able to replicate statistics of the observed tracer distribution that would be important in assessing the impact of oil releases in the middepth Gulf.

Key Points:
- Diapycnal mixing at middepth is enhanced along the continental slope
- Lateral homogenization of a passive tracer is also greatly enhanced
- A numerical simulation captured key statistics of observed tracer dispersion

Correspondence to:
J. R. Ledwell,
jledwell@whoi.edu

Citation:
Ledwell, J. R., R. He, Z. Xue, S. F. DiMarco, L. Spencer, and P. Chapman (2016), Dispersion of a tracer in the deep Gulf of Mexico, *J. Geophys. Res. Oceans*, *121*, 1110–1132, doi:10.1002/2015JC011405.

Received 21 OCT 2015
Accepted 6 JAN 2016
Accepted article online 12 JAN 2016
Published online 5 FEB 2016

1. Introduction

The Gulf of Mexico has been the subject of intensified study since the massive release of oil from the ruptured Deepwater Horizon well in 2010 (see *Lubchenco et al*. [2012] for an overview). As a part of that research effort, we have carried out a tracer release experiment starting along the northern slope of the Gulf not far from the rupture and at a depth of approximately 1100 m, similar to the depth of the deep plume from the rupture, as observed by *Camilli et al*. [2010]. The goals of the tracer experiment are to study the processes of dispersion in the middepth Gulf and to contribute to the improvement of numerical forecast models of circulation and dispersion. A practical motivation for this research is to provide better information to those interested in commercial development of Gulf resources, to regulators, and to those responding to the release of oil and other harmful substances into the Gulf at middepths.

Beyond these practical motivations, there is good reason to study processes of dispersion in marginal seas such as the Gulf of Mexico, in order to gain a better general understanding of the oceans. We shall show that mixing and stirring in the Gulf seem to be greatly enhanced along the continental slope, so much so that vertical mixing in the Gulf appears to be dominated by processes in this boundary region and lateral homogenization seems to be greatly facilitated in that same region. The northern slope of the Gulf offers very rough terrain for boundary currents making their way around the Gulf.

The forces driving these currents are many and varied. The Yucatan Channel current forms the Loop Current which intrudes to a variable extent into the Gulf, generating energetic eddies [e.g., *Sturges and Leben*, 2000; *Schmitz et al*., 2005; *Leben*, 2005; *Schmitz*, 2005] and topographic Rossby waves [e.g., *Oey and Lee*, 2002; *Hamilton*, 2009], both of which propagate from east to west. The eddies interact with the continental slope and rise of the northern Gulf [e.g., *Hamilton and Lugo-Fernandez*, 2001; *Hamilton and Lee*, 2005; *Schmitz et al*., 2005]. Tropical storms and hurricanes drive mixing, strong flows in the upper waters, and barotropic flows throughout the water column [e.g., *Jaimes and Shay*, 2010]; they also drive inertial waves that propagate into the deep water [e.g., *Shay et al*., 1998; *Oey et al*., 2008; *Jaimes and Shay*, 2010]. Forcing by winds proves to be particularly

important in our experiment because of the passage of Hurricane Isaac directly over the site about a month after the tracer release. An excellent summary of the physics of the Gulf of Mexico, with numerous references to earlier work, is given by *Sturges and Lugo-Fernandez* [2005].

Tidal currents in the Gulf, on the other hand, are relatively weak, as is the case in the Caribbean and in other marginal seas [*He and Weisberg*, 2002; *Kantha*, 2005]. Hence, the Gulf offers an interesting contrast to other oceanic regions in which kinetic energy is tidally dominated, especially for studies of mixing and the dynamics driving it.

A tracer release experiment can yield accurate, long-term, measurements of diapycnal mixing averaged over broad areas. Such experiments also inevitably yield unique information on lateral stirring and can in some cases add to knowledge of the general circulation in an area. Past tracer release experiments have confirmed estimates based on turbulence dissipation rates that the diapycnal diffusivity in the interior of much of the ocean is of order 10^{-5} m^2/s, for example in the North Atlantic pycnocline [*Ledwell et al*., 1998; *Banyte et al*., 2012], and in the southeastern Pacific sector of the Antarctic Circumpolar Current [*Ledwell et al*., 2011]. Diapycnal diffusivities have been found to be greatly enhanced, however, over rough topography [*Polzin et al*., 1997; *Ledwell et al*., 2000; *Watson et al*., 2013]. Proximity to the boundaries has also proven to be important to diapycnal mixing in smaller silled basins in the Southern California Borderland [*Ledwell and Hickey*, 1995; *Ledwell and Bratkovich*, 1995], and in the Baltic Sea [*Holtermann et al*., 2012]. Mixing in the overall basins, with areas on the order of 2000 km^2 at sill depth, appeared to be dominated by mixing within a few kilometer of the basin boundaries.

One of the questions addressed here is on the extent to which boundary-related mixing dominates basin-wide diffusion of tracers across submerged isopycnal surfaces in major marginal seas, such as the Gulf of Mexico, with a surface area of more than 10^6 km^2. Until the experiment described here, no such tracer release experiment had been undertaken in the Gulf of Mexico or other marginal sea, with the exception of the experiment in the deep basin in the eastern Baltic reported by *Holtermann et al*. [2012]. Furthermore, to our knowledge, prior to our experiment, no measurements of diapycnal mixing in subsurface waters have been undertaken in the Gulf at all, despite its unique dynamics.

With regard to along-isopycnal stirring and mixing, lateral dispersion of drifters in the surface waters of the Gulf of Mexico has been the subject of landmark studies [*LaCasce and Ohlmann*, 2003; *Poje et al*., 2014]. However, again, prior to our study, apparently no measurements of lateral dispersion and homogenization in the deep water of the Gulf have been undertaken. For that matter, studies of these processes in the deep ocean anywhere are quite rare. Nevertheless, the processes involved are important scientifically because they are poorly understood, yet must be parameterized in numerical models of ocean circulation. They are also important for practical reasons such as predicting pathways and concentrations of pollutants released at depth. Dispersion parameters at scales finer than the mesoscale have been estimated from tracer release experiments [e.g., *Ledwell et al*., 1993, 1998; *Sundermeyer and Price*, 1998; *Polzin and Ferrari*, 2004; *Sundermeyer et al*., 2005; *Smith and Ferrari*, 2009], but the dominant processes governing submesoscale dispersion in a given situation are not yet well understood. It is well established that mesoscale eddies tease a tracer into filaments which are separated by large swaths of tracer-free water until continual growth of the filaments by the mesoscale strain field finally causes them to start to fill the tracer-free areas of the overall region in which they reside [e.g., *Garrett*, 1983; *Haidvogel and Keffer*, 1984; *Ledwell et al*., 1998; *Sundermeyer and Price*, 1998]. *Ledwell et al*. [1993, 1998] found the width characterizing tracer filaments in the North Atlantic thermocline to be 2 orders of magnitude greater than expected from calculations of shear dispersion based on the known kinematics of the internal wavefield. Effective cross-streak diffusivities of order 2 m^2/s due to submesoscale processes were inferred from the observed tracer fields in that case [*Ledwell et al*., 1998; *Sundermeyer and Price*, 1998]. *Boland et al*. [2015] have estimated submesoscale diffusivities of 20 m^2/s in the Circumpolar Deep Water of the Antarctic Circumpolar Current in the southeast Pacific. The processes responsible for these diffusivities, at scales of 3–30 km, have not been definitively identified, though stirring by internal vortices has been proposed by *Polzin and Ferrari* [2004] and *Sundermeyer et al*. [2005], and dispersion by shears in the mesoscale velocity field coupled with diapycnal mixing has been proposed by *Smith and Ferrari* [2009]. We shall show here that homogenization by stirring and cross-filament mixing of the tracer released in the Gulf has been substantially faster than in the open ocean. This result is important for predicting pollutant concentrations in the deep Gulf, but identifying the dominant dispersive processes in this environment will require further research.

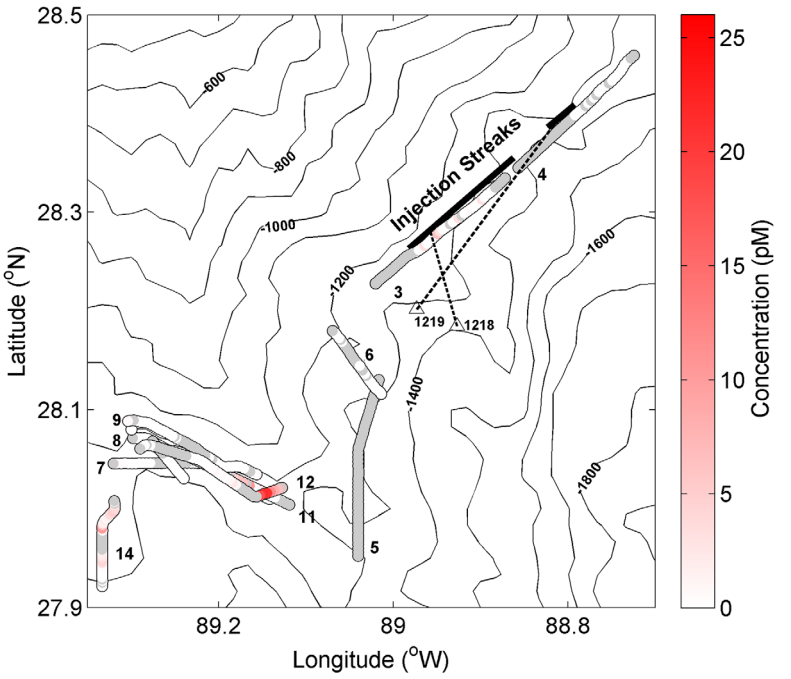

Figure 1. Overview of injection streaks (heavy black lines) and initial sampling tracks ("worms"). The white to red color shows tracer concentration in the syringes along the tracks; grey indicates syringes that failed to fill (1 p$M = 10^{-12}$ moles/L). The sampling tracks are numbered for reference to Figures 2 and 3. The black dashed lines show the displacements of two RAFOS floats released with the tracer, with a triangle at their final locations. The float marked 1218 drifted at the tracer depth for 65 h; float 1219 for 130 h. Isobaths are shown as fine black lines every 200 m. Bathymetry data throughout this paper are from the NOAA National Geophysical Data Center, U.S. Coastal Relief Model, available at the web site http://www.ngdc.noaa.gov/mgg/coastal/crm.html.

2. The Experiment

2.1. The Tracer

The tracer used for the experiment was 16.8 kg of trifluoromethyl sulfur pentafluoride, CF_3SF_5, a compound tested as a deep ocean tracer for long-term experiments by *Ho et al.* [2008]. This tracer is harmless and conservative in the marine environment, although it has a high global warming potential once in the atmosphere [*Sturges et al.*, 2000]. It is also highly electrophilic, making it detectable in quantities of less than 10^{-17} moles with a gas chromatograph equipped with an electron capture detector (GC/ECD).

2.2. Tracer Injection

The tracer was injected in a 25 km streak, albeit an interrupted one, on an isopycnal surface near 1100 m depth along the continental slope of the Gulf about 70 km southwest of the Deepwater Horizon site, on 28 July 2012 (Figure 1). The water masses of the Gulf are described, for example, by *Rivas et al.* [2005] and hydrographic characteristics along the injection path are listed in Table 1. The water at the injection depth lies below the salinity minimum at 800 m characterizing Antarctic Intermediate Water, and so is in a transition zone between this water and the more saline North Atlantic Deep Water that fills the deep Gulf and Caribbean Sea.

Table 1. Characteristics of the Tracer Injection

	Total or Mean	RMS Variation
Amount released	16.8 kg	
Length of the track (excluding the gap)	19.9 km (16.0 + 3.9 km for the two segments)	
Target σ_1	32.254 kg/m^3	0.8×10^{-3} kg/m^3
Pressure	1122 dbar	20 dbar
Temperature	4.733°C	0.0046°C
Salinity	34.9449	0.0003
Buoyancy frequency	2.5×10^{-3} s^{-1}	
Density ratio	−4.5 (stable)	
Height above bottom	152 m	28 m

The injection was performed with a system similar to that described by *Ledwell et al.* [1998, hereinafter LWL] in which a towed frame is maintained within ~1 m of the target isopycnal surface with a feedback system between a CTD on the injection sled and the ship's winch, while the tracer is sprayed at high pressure through 25 μm orifices to atomize it to speed dissolution.

Table 2. Tow Characteristics

Cast	Type of Cast	Mean σ_1 (kg/m^3)	Aux Cable Length (m)	Number of Samplers	Comments
1	Injection	32.2538		None	Injection tow
2	Test		50	21	No contamination found
3	10 h tow	32.2540	50	21	One sampler on sled; did not fill; lowest three samplers did not trip
4	10 h tow	32.2540	50	22	Two samplers on sled from here on
5	10 h tow	32.2540	50	22	
6	6 h tow	32.2539	50	22	
7	10 h tow	32.2539	50	22	Upper 10 samplers did not trip
8	10 h tow	32.2539	20	17	
9	3 h station		2	2	Spot samples; 3 h at constant pressure, 1190 dbar
10	10 h tow	32.2526	2	22	
11	Exploratory tow	32.2536	2	2	No tracer
12	10 h tow	32.2538	20	17	
13	Exploratory station		2	3	Spot samples-high tracer
14	5 h tow	32.2539	40	21	

The target potential density anomaly, referenced to 1000 dbar pressure, was 32.254 kg/m^3. The mean height above bottom of the injection was 150 m, and the vertical potential density gradient at the injection surface was approximately -4.8×10^{-4} kg/m^4. The interruption in the injection streak was due to concern that too much wire had been paid out, creating a risk that the package would hit bottom were the ship to slow down. Approximately 80% of tracer was released along the southwest segment of the path and 20% along the northeast segment.

2.3. Initial Condition

The distribution of the tracer was sampled with a towed system similar to that described by LWL, between 5 and 12 days after the release. This system includes a vertical array of integrating samplers spaced 4 m apart, and a sampling sled with CTD which was maintained on a target density surface, as for the injection. Samplers were deployed above the sled on the CTD cable and below the sled on an auxiliary cable (details are in Table 2). The samplers slowly drew approximately 850 mL of water into a metalized bag with a mechanically driven hydraulic system over a period of several hours as they were towed through the water. The system was towed along the tracks shown in Figure 1 for 5–10 h at speeds of approximately 0.5 m/s while the integrating samplers filled, having been tripped by mechanical messenger. At the center of the array was a carousel of 50 glass syringes programmed to fill sequentially, each one filling to approximately 60 mL during 12 min of the tow. The target density for the tows was not always the same as for the injection due to adaptation to the proximity of the bottom and to where the peak tracer appeared from earlier tows. Table 2 lists pertinent characteristics of the sampling tows.

The 50 syringe system was the same as described by LWL. The performance of this system was poor, however, due to persistent problems with alignment of the 50 port valve used in the system. Many syringes did not fill at all, while many others filled only partially. Nevertheless, the syringe data proved useful in guiding the sampling and in the analysis of the early lateral distribution of the tracer.

Concentrations in the syringes were determined by head-space analysis with the GC/ECD onboard the ship in the manner described by *Wanninkhof et al*. [1991]. Concentrations in the integrating samplers were also analyzed by head space after transferring sample water from the 850 mL bags in the samplers to 100 mL glass syringes. Uncertainties for 50 port syringe samples that filled properly and for the integrating samplers were a combination of 5% from volumetric uncertainty, and an uncertainty of about 0.2 f*M* due to GC noise (1 f$M = 10^{-15}$ moles/L). Volumetric uncertainties for 50 port syringes that did not fill all the way were greater than 5%.

Sampling was guided by two RAFOS floats deployed with the tracer and programmed to come to the surface after 2.7 days and 5.4 days. Both floats moved generally southward, and roughly parallel to isobaths at mean speeds of approximately 0.06 m/s. Lateral displacements of the floats during their missions are shown in Figure 1. Guidance was also provided by real-time numerical simulations of P. Chang and his group at Texas A&M University (TAMU), whose hindcast showed much of the tracer following the slope to the

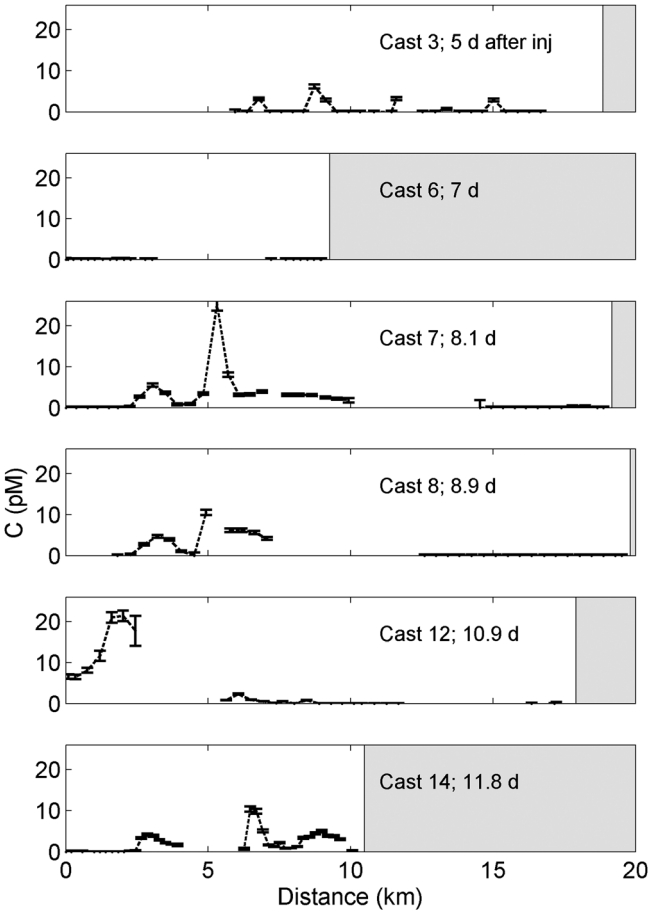

Figure 2. Fifty chamber sampler transects. The time since injection is indicated. The grey areas are beyond the sampling track. Gaps in the data indicate where the samplers failed to fill.

southwest, and by R. He and his group at North Carolina State University (NCSU), whose hindcast showed the tracer moving south, but a bit more offshore. Flow along the topography to the southwest was also estimated by *Weisberg et al*. [2011] for the time of the Deepwater Horizon blowout.

The tracer appeared to be distributed in a band along the continental slope southwest of the injection area (Figure 1), although time did not allow a thorough survey. Tows 7–12, though in the same geographical location, are believed to have sampled different water each day because of the estimated along-isobath flow at the level of the tracer. Transects from the 50 syringe sampler showed the tracer to be distributed in streaks with a characteristic width on the order of 3 km (Figure 2). Six vertical profiles with significant tracer concentrations were obtained from the integrating samplers (Figure 3). The upper tails of these profiles were delimited for all the tows, with the exception of Tow 7 for which the upper part of the sampler array did not trip. Except for Tows 3 and 6, the lower tails of the profiles were not delimited, due to insufficient coverage by the array. The impact of these shortcomings turns out to be small, as will be discussed in section 4.

2.4. Four Month Survey

The tracer patch was surveyed again in December 2012, roughly 4 months after the tracer release (Figure 4) with a conventional CTD/rosette system with twenty-two 4 L Niskin bottles. One liter glass bottles were filled from the Niskin bottles and concentrations were analyzed by purging the gases from a 270 mL aliquot of sample with nitrogen onto a trap at −60°C to −70°C, and releasing the gases from the trap into the GC system. Uncertainties were a combination of 2% of the concentration and a noise floor for this cruise of 0.1 f*M*. Details of the system were mechanically the same as described by *Law et al*. [1994]. The GC columns were chosen following guidance from W. Smethie [see also *Ho et al*., 2008], with parameters (Table 3) selected for CF_3SF_5 rather than SF_6.

The tracer search was guided by a third RAFOS float released during the injection, whose trajectory, like those of the earlier floats, was along the continental slope to the southwest (Figure 5). Guidance was also provided by the South Atlantic Bight and Gulf of Mexico (SABGOM) regional circulation model at North Carolina State University, described in section 3. The tracer patch was expected from the float trajectory to be centered between 90°W and 91°W, not accounting for retardation of the float by bumping along the bottom after suffering damage during Hurricane Isaac a month into its mission. Numerical floats in the real-time simulation also moved largely to the west along the slope, but most moved faster than the RAFOS float, being clustered near 93°W and spread along the slope to southern Texas and Mexico. Another patch of these floats moved into the interior and appeared to have circulated around Eddy "B" in Figure 4, located near 26°N, 89°W. As it turned out, high tracer concentrations were indeed found between 90°W and 92°W

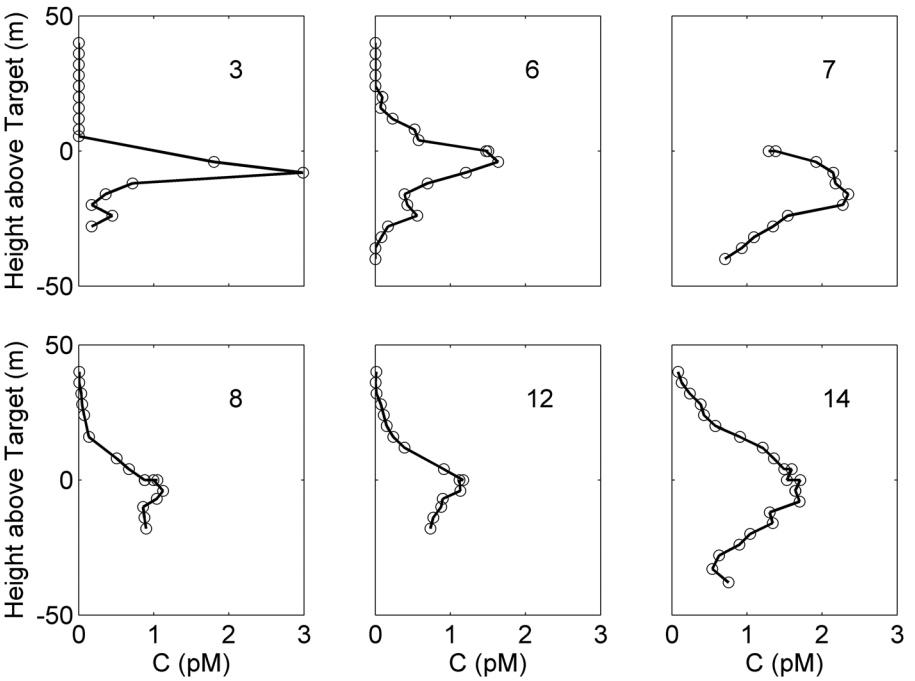

Figure 3. Vertical concentration profiles from the integrating samplers during the initial survey. The cast number is indicated.

along the slope, but very little tracer was found to the west of the anticyclonic Eddy "A" in Figure 4, centered near 26°N, 92°W. Rather, much of the tracer was found in the interior of the Gulf with high concentrations found at the limits of the survey from 92°W to nearly of 87°W.

Most of the stations of the 4 month survey were occupied in a "radiator" pattern in a series of cross-slope transects, about 70 km apart in the along-slope direction (Figure 4). Station spacing along these transects started at 11 km in the west and increased to 18.5 km as the spatial covariance, on one hand, and the size of the area to be covered to delimit the tracer, on the other, became apparent. The along-transect length scale of the column integral of tracer by this time was on the order of 50 km (Figure 6).

Individual vertical profiles of the tracer showed great variety (Figure 7). Profiles near the continental slope were relatively simple in shape but were generally broader than the often multipeaked profiles found in the interior. Multiple peaks indicate interleaving of low tracer water with high tracer water, a process which is likely at the edges of the tracer patch or at the edges of streaks within the tracer patch. An average over many profiles, in density space, removes most of this effect, as will be seen in section 4.

The background color in Figure 4 is a map of the tracer constructed with objective analysis (or Kriging) based on the station data and using the covariance function shown in Figure 15. This map is highly smoothed, masking the streakiness discussed in sections 4 and 5. The map accounts for 71% of the tracer released. Figure 4 shows tracer was very likely beyond the region surveyed, especially to the east and south. Also, our sampling may have missed high concentrations within the region surveyed due to streakiness (section 4).

2.5. Twelve Month Survey

The tracer field was surveyed again in August 2013, approximately12 months after the release (Figure 8), from R/V *Pelican* using a CTD/Rosette system with 12 L Niskin bottles. Tracer profiles were found to be rather smooth and the density range occupied by the tracer was found early to be predictable (Figure 9) and so only 12–14 of the Niskin bottles were tripped in the layer apparently occupied by the tracer. The others were used for sampling salinity and other constituents over the full water depth in order to add to the rather scanty hydrographic database of the deep Gulf. Analysis of these more general geochemical data must await a future communication.

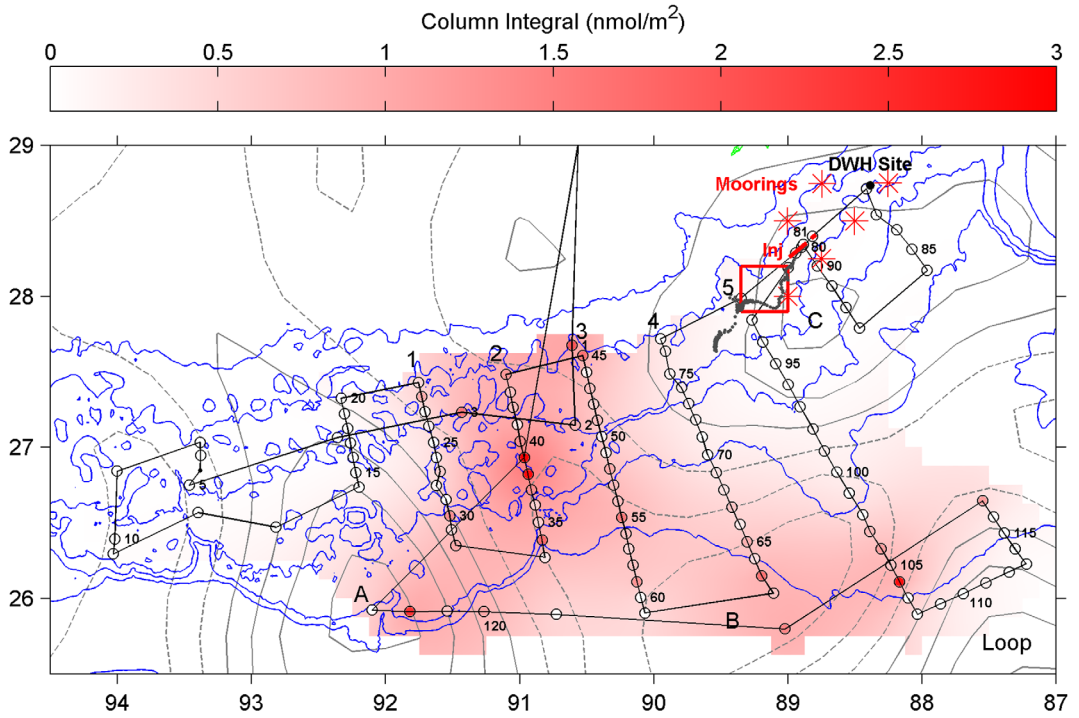

Figure 4. Four month survey map. The circles along the black cruise track are colored according to the column integral of tracer found, with selected stations numbered for reference. The diffuse white to red colored background is a highly smoothed objective map based on these station data (see text). Column integrals along transects labeled 1–5 at their northern ends are plotted in Figure 6. The abscissa and ordinate are longitude (°W) and latitude (°N). Isobaths are plotted in blue every 500 m, deepening toward the south. The southern tip of the Louisiana coastline is barely visible in green near 29°N, 89.4°W. The Deepwater Horizon site (DWH) is at the black dot in the northeast corner. The red box near 28°N, 89°W, delimits the map of the injection, shown here as a red line, and initial sampling shown in Figure 1. The mooring locations for the GISR experiment are shown as red asterisks. The serpentine line made of black dots is the trajectory of RAFOS float 1215, released with the tracer and shown in detail in Figure 5. Sea surface height on 16 December 2012 is contoured in grey at 5 cm intervals, with negative contours dashed. "A" labels a prominent anticyclonic eddy, and "B" and "C" label weaker cyclonic and anticyclonic eddies, respectively. The tip of the Loop Current is in the southeast corner. Analyzed altimetry data are from the Colorado Center for Astrodynamics Research, and are viewable at the site http://eddy.colorado.edu/ccar/data_viewer/index.

The samples were analyzed on board with the GC/ECD as described above. The volume of water sparged was increased to 655 mL. For Stations 1–11, concentration uncertainties for the GC were again nearly 0.1 f*M* (1 standard deviation). After Station 11 concentration uncertainties were lowered to approximately 0.02 f*M* by eliminating noise with extensive baking of the GC detector and associated tubing.

Stations were widespread, although the ship time available did not allow a complete survey. Eddy "A" by this time had weakened and moved west to about 26°N, 95°W where concentrations were low. Very little tracer was found within the Mexican EEZ (Figure 8). High concentrations were still found in the north along the slope, as for the 4 month survey, and were also found in the east. Again, a highly smoothed objective map of the tracer is shown in the background in Figure 8. The fraction of tracer represented in the map is 53% of the amount released. This shortfall is discussed in section 4.

Table 3. GC/ECD Analysis Operating Parameters

Precolumn	0.1 m long × 0.83 mm ID SS Molecular Sieve 5A, 80/100 mesh
Main columns	First: 1.2 m × 0.83 mm ID SS Unibeads 2S
	Second: 1.8 m × 0.83 mm ID SS, Carbograph, 1% AT1000
Column temperature	70°C; precolumn heated to 95°C during backflush
Carrier	UHP nitrogen at 25–30 mL/min
GC	Shimadzu GC8A with Electron Capture Detector
Detector temperature	330°C
Detector current	2.0 nA
Cold trap	Unibeads 2S at −60 to −70°C
Sparge volume	260 mL (655 mL for the 12 month survey)
Sparge flow	UHP nitrogen at 150 mL/min for 4 min

3. Numerical Simulation

Numerical simulations of the Gulf circulation have been a continuous community effort since the late 1970s. Various circulation aspects in the Gulf have been examined using models with different

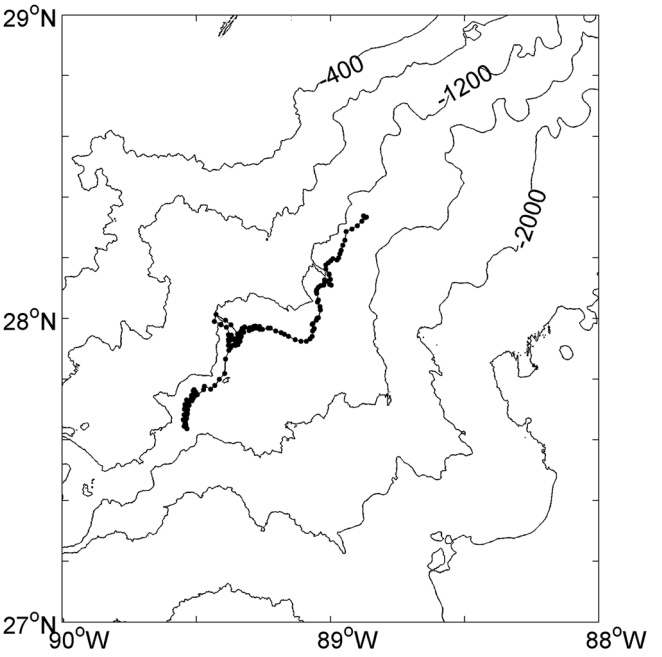

Figure 5. RAFOS 1215 trajectory. Deployment was at the NE end, during the injection on 28 July 2012. Three fixes a day were obtained (dots). The excursion to the NW two thirds of the way through the trajectory started on 29 August, shortly after landfall of Hurricane Isaac on the Louisiana coast. During this excursion, the float hit the bottom on 1 September and apparently was damaged, because the pressure record indicated that after this time the float was hopping along the bottom.

complexity and realism, including two-layer and reduced gravity models [e.g., *Hurlburt and Thompson*, 1980] in the early stages and realistic, three-dimensional primitive equation barotropic and baroclinic models in last two decades [e.g., *Oey*, 1996; *Morey et al.*, 2005; *Chassignet et al.*, 2009; *Halliwell et al.*, 2014, among many others]. In this study, the dispersion of the tracer was simulated with the SABGOM circulation model. The model is described in detail elsewhere [*Hyun and He*, 2010; *Xue et al.*, 2013, 2015]. Briefly, it is based on the Regional Ocean Modeling System (ROMS) [*Shchepetkin and McWilliams*, 2005; *Haidvogel et al.*, 2008] with horizontal resolution of approximately 5 km, and with 36 vertical levels. Conditions at the open boundaries are from the 1/12° daily North Atlantic Hybrid Coordinate Ocean Model (HYCOM/NCODA) [*Chassignet et al.*, 2007], superimposed with eight major tidal harmonics derived from a regional tidal solution using the Oregon State University Tidal Data Inversion Software (OTIS) [*Egbert and Erofeeva*, 2002]. Surface stress and buoyancy forcing was from the 3 hourly, 32 km resolution, North American Regional Reanalysis (NARR, http://www.esrl.noaa.gov/psd/). The method of *Mellor and Yamada* [1982] was used to compute vertical turbulent mixing. Harmonic horizontal viscosity with a constant value of 100 $m^2\ s^{-1}$, and the quadratic drag formulation with a drag coefficient of 3×10^{-3} for the bottom friction specification were adopted.

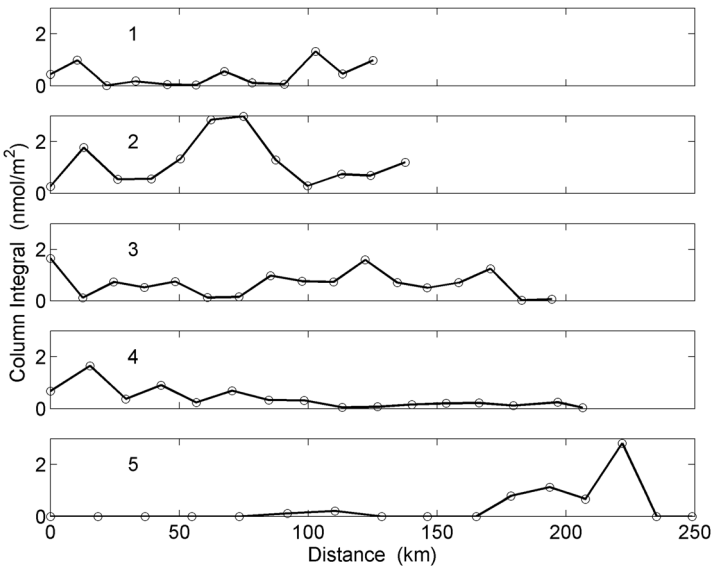

Figure 6. Tracer column integral along transects 1–5 indicated in Figure 4. Distance is measured from the northernmost station.

Temperature and salinity were relaxed to HYCOM/NCODA water mass fields with a 30 day time scale. This procedure allows the model to evolve according to its own high-resolution dynamics, while incorporating the low-frequency HYCOM model prediction that assimilates routine satellite surface temperature, sea surface height, and available subsurface hydrographic observations. Extensive model-data validations have shown that SABGOM provides a realistic circulation hindcast in terms of resolving mesoscale processes in the Gulf, such as shelf circulation, the Loop Current, and Loop Current eddy dynamics [*Hyun and He*, 2010; *Xue et al.*, 2013, 2015; *North et al.*, 2011, 2015]. We are

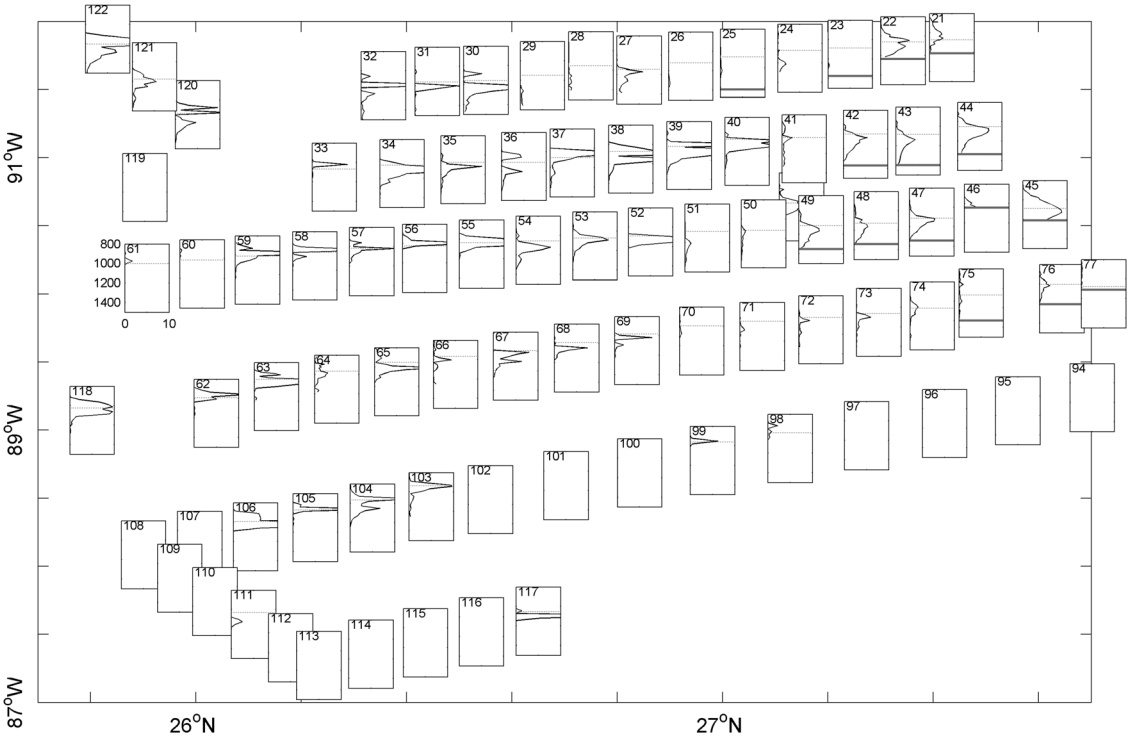

Figure 7. Vertical concentration profiles, 4 month survey. The insets are placed approximately geographically, with the continental slope (and north) to the right, with latitude on the horizontal axis and longitude on the vertical axis of the overall figure. The axes of each inset are the same and are quantified in inset 61, with depth from 800 to 1500 m on the vertical axes, and concentration from 0 to 10 f*M* on the horizontal axes (1 f*M* = 10^{-15} moles/L). The depth of the target density is shown in each figure as a dotted line. The bottom depth, when less than 1500 m, is shown by the thick grey line (figures in the upper right).

examining the model skill in resolving point observations collected by an array of ADCP current meters and drifters during the same time period. The model is able to reproduce important statistics of these observations, but further model refinements (such as adopting higher resolution) are needed to enhance model performance. We will report this finding, along with an analysis of submesoscale circulation dynamics in a future correspondence.

Numerical passive tracer was advected in the simulation with the Multidimensional Positive Definite Advection Transport Algorithm (MPDATA) [*Smolarkiewicz*, 1984]. The sigma coordinates of a terrain following model, as used here, can introduce vertical fluxes even when density surfaces are flat in Cartesian coordinates. To help remedy this, explicit horizontal diffusivity was set to zero for the simulations. However, processes such as numerical diffusion coupled with shear can certainly play a role in the evolution of the simulated tracer distribution, especially at small lateral scales. *Marchesiello et al*. [2009] discussed this issue in detail and concluded that spurious diapycnal diffusion is associated with all advection schemes in sigma models, particularly the third-order upwind advection scheme. This is one of the reasons we chose to use the MPDATA advection scheme. The other reason is that this positive definite scheme is most suitable for tracer simulation.

The tracer was released in the model in the grid boxes laterally closest to the initial tracer streak, and vertically distributed over four layers ranging in depth from 999 to 1217 m with an average depth of 1103 m. Maps of the tracer column integral from the simulation at 4 and 12 months after release are shown in Figures 10 and 11, respectively, along with the observed column integrals. A movie of the simulation is in the ancillary file sabgom_tracer.mov. In this movie, it can be seen that branches of the tracer patch moved along the U.S. continental slope both to the west and to the east of the release location. The western branch eventually made its way south and then east along the Mexican continental slope. The eastern branch made its way toward the Yucatan Strait and the Florida Strait and tracer passed through those straits to leave the Gulf. However, the highest concentrations and the majority of the tracer stayed in the northeastern region of the Gulf, i.e., east of 90°W and north of 25°N. This main part of the patch moved west at first but then back to the east in the simulation.

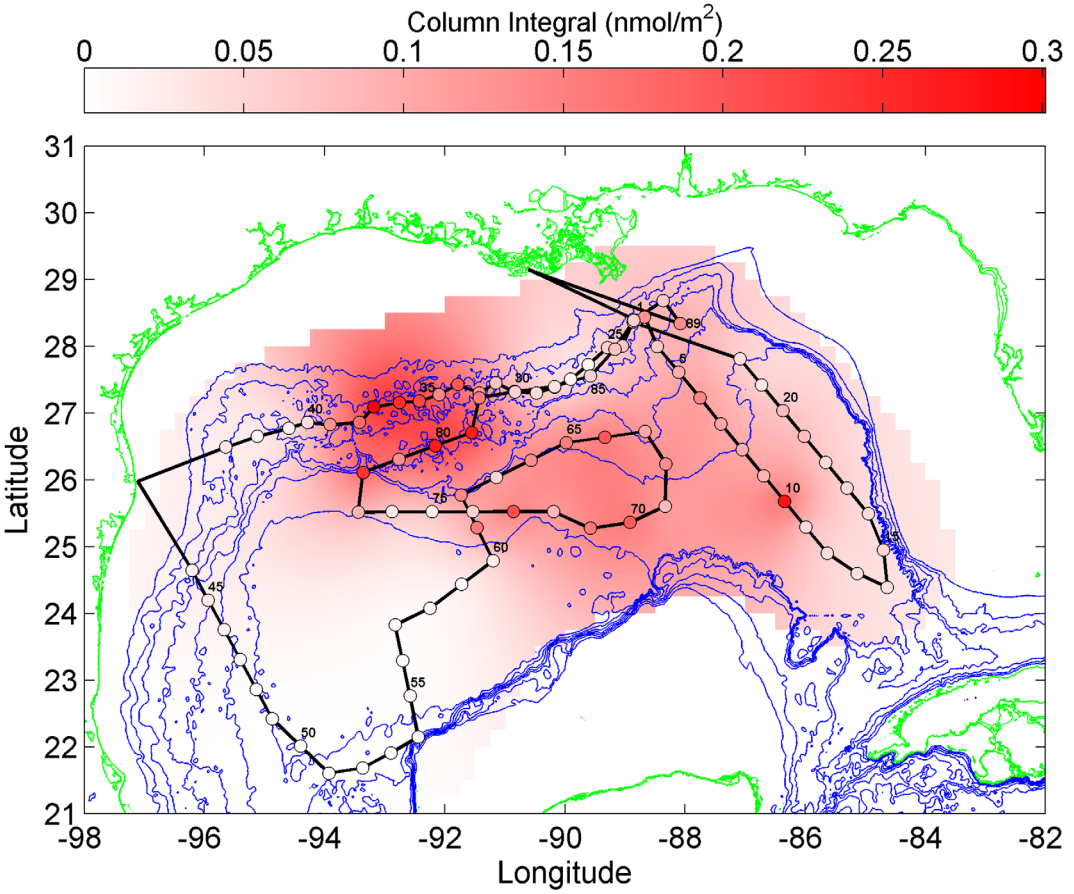

Figure 8. Twelve month survey map. The circles along the black cruise track are colored according to the column integral of tracer found, with selected stations numbered for reference. The diffuse white to red colored background is a highly smoothed objective map based on these station data (see text). Isobaths are plotted in blue every 500 m, and the coastline is green.

As might be expected, due to propagation of model errors over such long times and the patchy nature of the tracer distribution, there are many differences in a point by point comparison between simulated and observed tracer fields. Displacements of this scale could have a myriad of origins, but one likely source is energetic mesoscale meanders and eddies within the gulf. These motions exist in the present physical model (grid spacing of 5 km) but cannot be deterministically replicated. Broadly speaking, at 4 months the simulated tracer seems to lie to the east and the north of the observed tracer (Figure 10). At 12 months, the simulated tracer may again be more concentrated to the east of observed tracer. Particularly notable is that the simulation did not capture the relatively high tracer concentrations observed along the continental slope near 90°W (Figure 11). However, as will be discussed in the next section, some important statistics of the simulated tracer distribution do match the observations. As will also be seen, details that are resolvable in the simulation but not in the sparsely spaced observations, help interpret the latter.

4. Analysis

4.1. Diapycnal Diffusivity—First 4 Months

Diapycnal diffusivities may be estimated from the progression of the distribution of the tracer in density space with time. There are two confounding difficulties with the current experiment. A relatively minor one is that the diapycnal distribution at densities greater than the target density of the release was not well bounded (Figure 3), due to the short length of the lower part of the sampling array. This difficulty turns out to be minor because the least squares procedure described below calls for virtually no tracer deeper than the range sampled during the initial survey, though it is free to call for as much tracer as needed there to minimize the cost function.

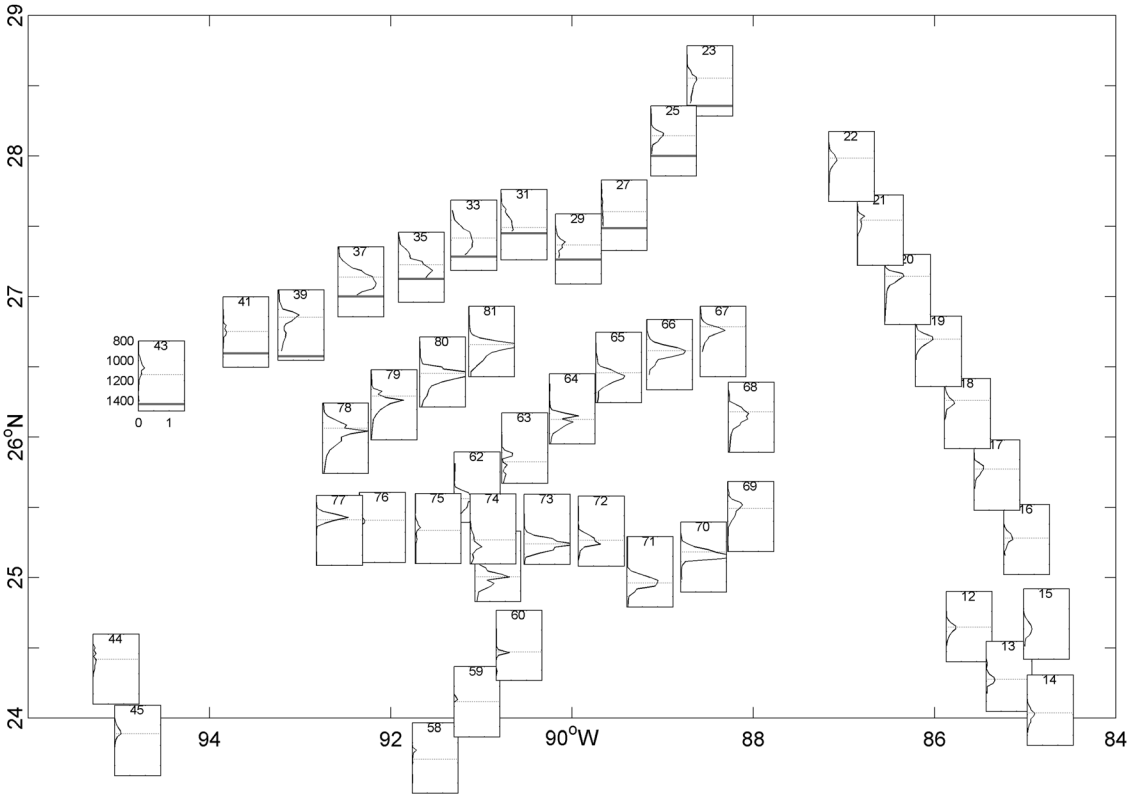

Figure 9. Vertical concentration profiles, 12 month survey. Some closely spaced profiles are omitted for clarity. Profiles 1–11 are not plotted due to GC noise. The insets are placed approximately geographically. The axes of each inset are the same and are quantified in inset 43, with depth from 800 to 1500 m on the vertical axes, and concentration from 0 to 1.5 f*M* on the horizontal axes. The depth of the target density is shown in each figure as a dotted line. The bottom depth, when less than 1500 m, is shown by the thick gray line (figures along the northwest edge).

The other confounding difficulty, which however adds interest to the experiment, is that mixing was apparently much greater near the continental slope than away from it. The tracer release approach is not a very sharp tool in differentiating between boundary mixing and interior mixing because one cannot control or

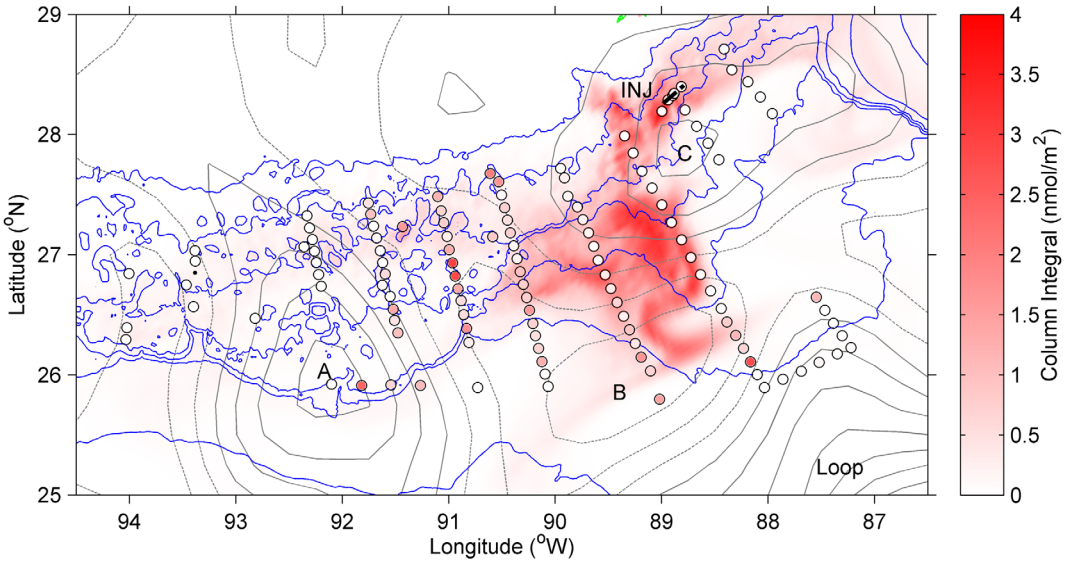

Figure 10. Numerical simulation of the tracer column integral 4 months after release (red) superposed on the observed column integral from the stations occupied at 4 months (circles filled with red from the same palette). Isobaths are shown every 500 m. Sea surface height anomaly contours are shown in grey at 5 cm intervals, solid for positive anomalies, dashed for negative. Eddies A, B, and C and the Loop Current are indicated.

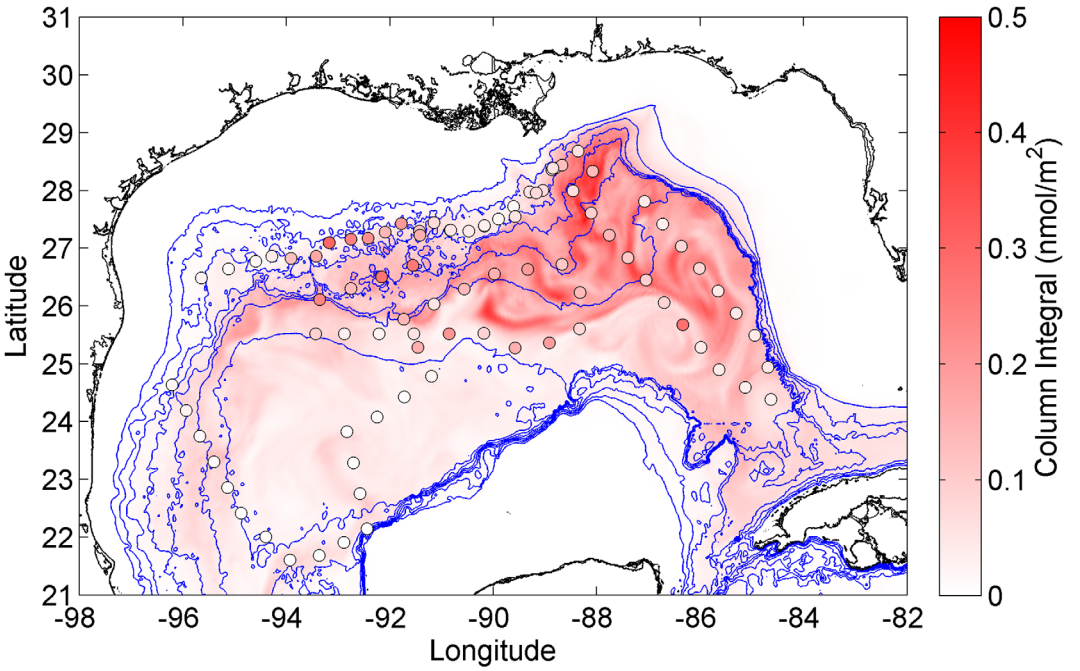

Figure 11. Numerical simulation of the tracer column integral 12 months after release (red) superposed on the observed column integral from the stations occupied at 12 months (circles filled with red from the same palette). Isobaths are shown every 500 m (blue); the coast is shown in black.

know the amount of time the tracer has spent in the respective regions. However, the tracer measurements do allow useful limits to be placed on the diffusivities in the two regions.

To this end, the stations have been divided into two groups, a "boundary" group comprising all the stations shoreward of the 1500 m isobath, and an "interior" group comprising those stations seaward of this isobath. The boundary stations are those in Figure 7 for which the bottom appears on the profile subplots as a thick gray band. The choice of this dividing isobath is somewhat arbitrary, but it does separate the simple broad peaks near the slope from the narrower interior peaks. The means of these two groups (Figure 12) were computed as a function of density and then converted to depth through the mean depth/density relation for the interior stations, shown in Figure 13. The mean boundary profile is much broader than the mean interior profile, in this common coordinate, especially in the deep wing of the profile, implying that mixing was enhanced near the boundary. Discontinuities in the boundary profile are due to profiles dropping out of the mean because of the presence of the bottom.

A diapycnal diffusivity of 1.3×10^{-4} m^2/s is estimated by applying a 1-D diffusion model to the change from the initial mean profile to the mean interior profile for the 4 month survey, following the method of LWL (Figure 12). The least squares procedure of this model selects concentrations in the initial deep tail that fall off rapidly at depths greater than 40 m below the target density surface, the limit of the observations. As noted earlier, the implication is that the observed deep tracer at 4 months does not indicate that very much tracer resided in the unsampled region below −40 m during the initial survey.

Application of the same 1-D diffusion model to the evolution from the initial mean profile to the mean boundary profile gave an estimate of the diffusivity for the boundary region of 4×10^{-4} m^2/s, though with a much poorer fit than for the mean interior profile (Figure 12). The interpretation of this result is not straightforward, because: the diapycnal diffusivity no doubt depends on distance from the boundary; the categorization of "boundary" is arbitrary; and how close to the boundary the tracer in each profile had been since the release is unknown. The difference between the interior and boundary result for the diffusivity is strong evidence, however, for significant enhancement of mixing over the slope.

The same caveats as above apply to the diffusivity of 1.3×10^{-4} m^2/s inferred from the mean interior profile. This is not to be taken as the diffusivity in the interior, because most of the tracer probably spent some time in the boundary region. The evolution from 4 to 12 months, to be discussed next, gives a much smaller

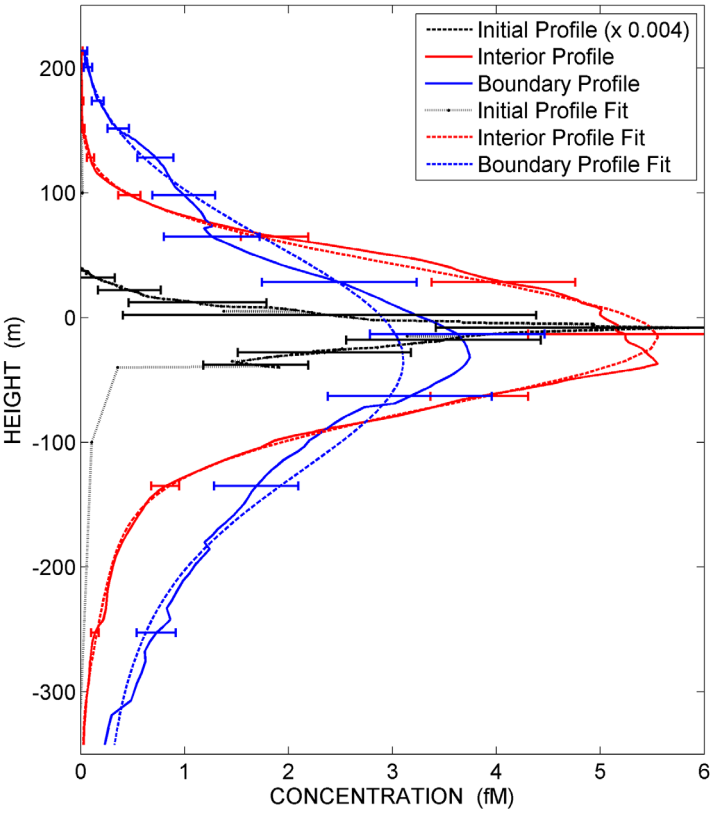

Figure 12. Initial and 4 month mean vertical profiles. Height is relative to the target isopycnal surface. The dashed black curve is the mean of the individual profiles from the initial survey, 5–12 days after release, multiplied by 0.004 to graph it with the other profiles. The red and blue curves are the mean of the interior and boundary profiles, respectively, from the 4 month survey. The black dotted and dashed red curves are the least squares fit to the initial profile and the 4 month interior profile, respectively, from the 1-D diffusion model, with diffusivity 1.3×10^{-4} m^2/s. The dashed blue curve is the least squares fit from the 1-D model for the boundary profile with diffusivity 4×10^{-4} m^2/s.

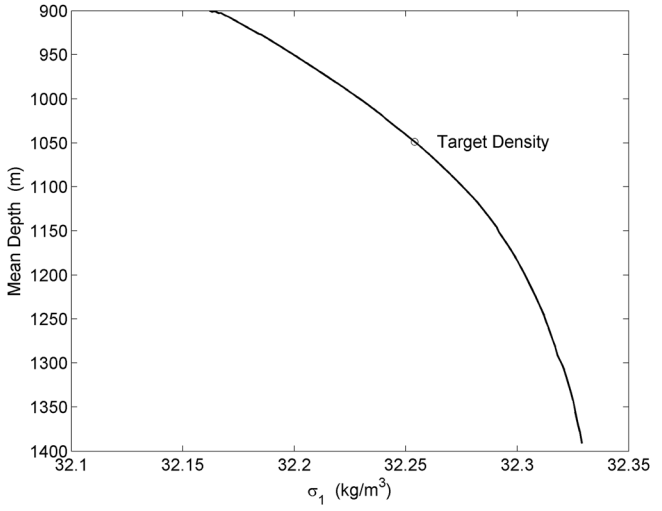

Figure 13. Mean density profile for the interior stations from the 4 month survey. The reference pressure for potential density is 1000 dbar. This curve is used to convert all of the mean profiles in density space to mean profiles in height above the target surface.

diffusivity for the interior for that time period. Because of the ambiguity in where the tracer has been, we do not assign error bars to the diffusivities inferred for this first time period.

4.2. Diapycnal Diffusivity—Four to Twelve Months

The mean of all the profiles from the survey in August 2013, 12 months after release, was almost indistinguishable from the mean interior profile at 4 months (Figure 14; the 4 month profile was shifted up by 10 m, assuming a CTD calibration shift). Application of the 1-D diffusion model of LWL yields a diapycnal diffusivity of $(0.15 \pm 0.05) \times 10^{-4}$ m^2/s, an order of magnitude smaller than found for the period between the initial survey and the 4 month survey, and similar to values found from tracer release experiments in the interior of the open ocean [*Ledwell et al.*, 2011; LWL]. Inclusion of a vertical gradient in the diapycnal diffusivity, which is allowed by the method, does not improve the fit significantly. The result for the diffusivity is not sensitive to the shift of 10 m that was applied to the 4 month mean profile, but the cost function is reduced by this shift. Uncertainties reported here are subjective estimates from the behavior of the cost function used in the least squares procedure, and assessment of the difference between observed and modeled mean profiles.

4.3. Spatial Autocorrelation

Mapping a tracer cloud for an experiment such as ours is very much like mapping mineral veins in the mining industry. Hence, we borrow statistical techniques from that field, and in particular the variogram [e.g., *Journel and Huijbregts*, 1978]. A normalized spatial covariance based on the

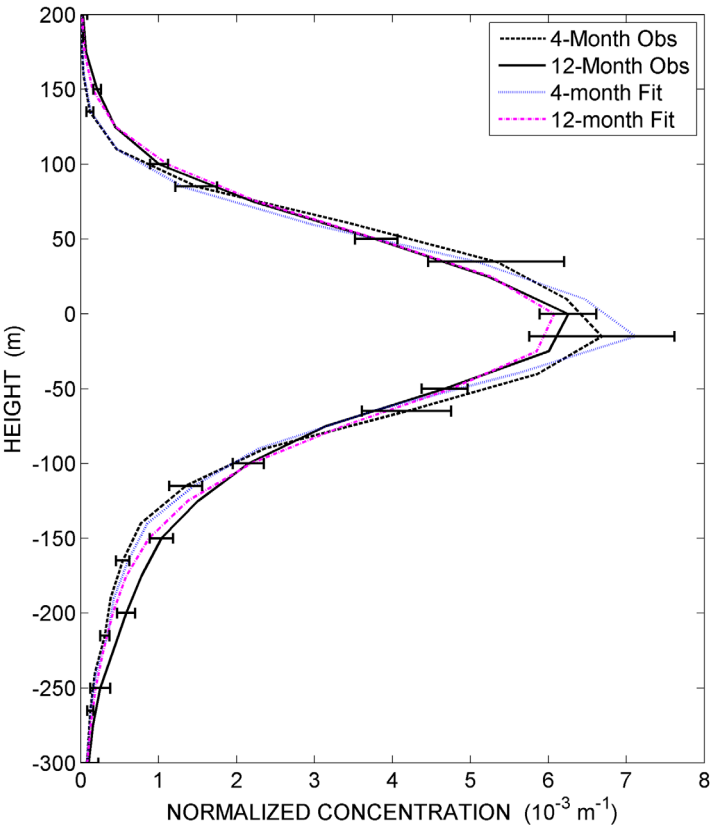

Figure 14. Mean of the interior profiles at 4 months, shifted up 10 m (dashed black curve), of all the profiles at 12 months (solid black), and least squares fit from the model for the 4 month mean (dotted blue) and the 12 month mean (dash-dotted magenta). Height is relative to the target isopycnal surface.

variogram, which we shall call the spatial autocorrelation, is:

$$A_k \equiv 1 - \frac{\sum_{m=1}^{N} \left\{ \sum_{n=1}^{N_m^k} (I_m - I_n)^2 \right\}}{\sum_{m=1}^{N} \left\{ \sum_{n=1}^{N_m^k} (I_m^2 + I_n^2) \right\}} \quad (1)$$

where N is the number of stations, I_m is the column integral of tracer at station m, and the sums are over all pairs of stations separated by a distance r in distance bin k defined by $r_k \le r < r_k + \Delta r$, where Δr is the bin size. That is, $\sum_{n=1}^{N_m^k}$ is a sum over those stations whose distance from station m is in the kth bin. To maintain symmetry in (1), all pairs are counted twice in both the numerator and the denominator. A_k takes on the value 1 at distance 0, and tends to decrease with increasing distance, but is always positive. Pairs whose members are both zero do not contribute to the sums at all, which is an advantage over the spatial autocorrelation defined in LWL.

This spatial autocorrelation is shown in Figure 15 for the observations and, in the case of the 4 and 12 month surveys, for the SABGOM simulation sampled at the same locations as the observations. Error bars were estimated by the jackknife method [*Effron and Gong*, 1983]. The magnitude of the abrupt drop in the autocorrelation between 1 at zero distance and the value in the first distance bin gives coarse information on the magnitude of unresolved small-scale features of the tracer patch, such as filament width. The much greater length scale of the drop beyond the first bin seems to be on the order of the overall size of the tracer patch rather than of details within it.

Figure 15 includes, for the 4 and 12 month surveys, exponential fits to the spatial autocorrelation that were used in making the smooth color maps of the tracer field in Figures 4 and 8, using the method of objective analysis [*Bretherton et al*., 1976], or, equivalently, simple Krigging with a nugget effect [e.g., *Journel and Huijbregts*, 1978]. These maps do not at all capture the interesting filamentation that is certainly there, as exemplified by the numerical simulations discussed in the next subsection.

4.4. Streakiness

The maps of Figures 10 and 11 show the tracer in the SABGOM numerical simulation to be distributed in broad streaks created by the stirring of the eddy field. The same phenomenon has been seen in many past simulations of tracer dispersion in the ocean [e.g., *Haidvogel and Keffer*, 1984; *Sundermeyer and Price*, 1998; *Lee et al*., 2009; *Tulloch et al*., 2014]. This behavior was described elegantly by *Garrett* [1983]. The actual tracer distribution was presumably arranged in streaks qualitatively similar to those in the simulation, but the resolution and coverage of the sampling at 4 and 12 months were not at all adequate to reveal streaks directly.

As noted in section 2, the initial survey found the tracer distributed in features a few km across (Figure 2). It appears that individual streaks were resolved by the 50 chamber sampler, although spatial aliasing of

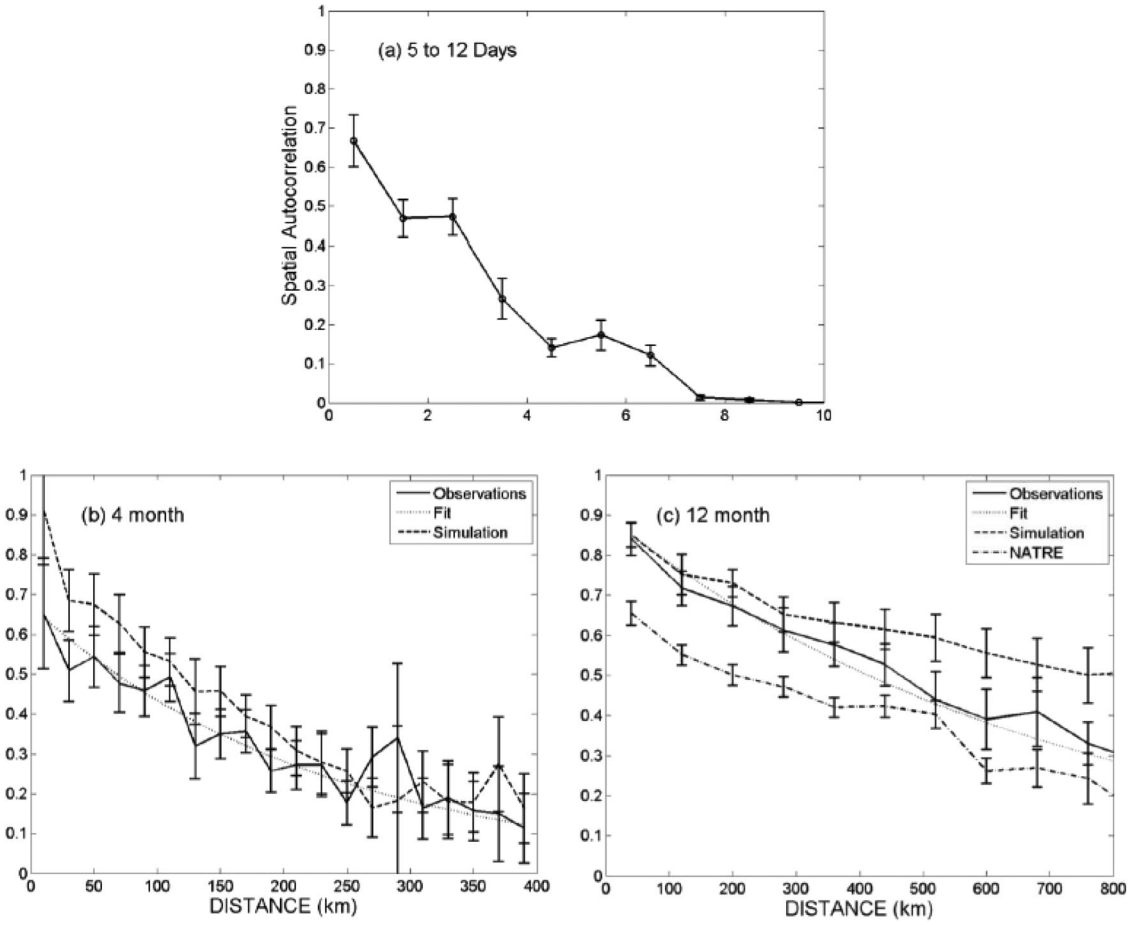

Figure 15. Spatial autocorrelation A_k of concentration at the 50 chamber sampler (a) for the initial survey 5–12 days after injection, (b) for the column integral of tracer for the 4-month survey for the observations (solid), and (c) for the simulation sampled at the same locations as for the 12-month survey (dashed), all from equation (1). The same function for the tracer release in the North Atlantic (LWL) at 12 months after release is plotted as a dash-dotted line in Figure 15c. The dotted lines in Figures 15b and 15c are the autocorrelation functions used in the color tracer maps in Figures 4 and 8, respectively.

streaks at smaller scales than resolved is always likely. The spatial autocorrelation drops rapidly with distance, falling to 0.65 in the first bin, centered at 0.5 km, and falling to less than 0.2 beyond 4 km (Figure 15a). It is clear that at this early time in the experiment sampling with a towed system rather than spot sampling with vertical CTD/Rosette casts was advantageous, if not absolutely necessary.

By the time of the 4 month cruise, the tracer distribution seemed to be coherent over scales of tens of kilometers (Figure 6), so that sampling by CTD/Rosette was effective. The autocorrelation again drops to 0.65 in the first bin, which, however, is now 20 km wide, and drops to around 0.2 beyond 250 km, the peak with large error bars at 290 km notwithstanding (Figure 15b). The autocorrelation for the SABGOM simulation at this time drops only to 0.9 in the first bin, versus 0.65 for the real tracer, suggesting that the real tracer streaks were narrower than those evident in the simulation in Figure 10. The two autocorrelations converge near 250 km, suggesting that the overall length scales of the observed and simulated patches were similar.

At 12 months, the autocorrelation for both the observed and simulated tracer patches drops to around 0.85 in the first 80 km wide bin (Figure 15c). Filaments are much broader, or are on their way to merger by this measure, compared with 4 months, and the variability at these scales seen in the simulation (Figure 11) is perhaps a guide to scales of variability for the actual tracer. Beyond the first distance bin, however, the autocorrelation falls off much faster for the observations than for the simulation (Figure 15c). This is perhaps due to the simulated tracer more nearly filling the Gulf than appears to be the case in the observations: column integrals in the southwest half of the Gulf were 10–20% of the maximum values in the simulated field (Figure 11), while the sparse sampling of the survey found virtually no tracer in this region.

4.5. Mass Budgets

As noted earlier, the fraction of tracer integrated over the objective maps of Figures 4 and 8 for the 4 and 12 month surveys was 72% and 53%, respectively. There is considerable uncertainty in the integral of maps like these, but by any means of integration there appear to be shortfalls of this order in the surveys. Loss over the 800 m deep sill in Florida Strait seems very unlikely. Loss through the Yucatan Channel between 4 and 12 months is possible, however, as shown by moored current meter arrays [*Ochoa et al*., 2001; *Bunge et al*., 2002; *Sheinbaum et al*., 2002; *Candela et al*., 2002; *Badan et al*., 2005; *Rivas et al*., 2005]. *Sturges* [2005] has shown a three-layer system below 800 m, with water flowing into the Gulf between 800 and 1100 m and between about 1900 m and the bottom, but flowing out of the Gulf to the south between 1100 and 1900 m. Observations indicate an outward volume flow of about 1 Sv (1×10^6 m^3/s) [*Rivas et al*., 2005; *Sturges*, 2005], while circulation models suggest a somewhat larger flow of order 3 Sv, with considerable variability [*Cherubin et al*., 2005]. In the SABGOM simulation, only 2% of the tracer leaves the Gulf by this route by 12 months, with most of the escape occurring between 4 and 12 months. We can only speculate on how much of the real tracer passed into the Caribbean, but it does not seem that this route can account for the missing tracer.

Part of the explanation for the shortfalls in the mass integrals lies in the spatial autocorrelations discussed above, the streakiness of the tracer making it harder to find. Also, high concentrations found around the geographical limits of the 4 month survey indicated that we missed tracer beyond these boundaries. At 12 months, the observations found no tracer in the southwest half of the Gulf, but there is a large unsampled area there, and in fact there are large spaces between all the sampling lines. Hence, perhaps the best explanation for the shortfall of the 12 month survey is that much of the tracer was far from the sparsely spaced track lines.

4.6. Distribution of Concentrations

A histogram of the concentrations found during the initial survey in the 50 chamber sampler is shown in Figure 16a, with a bin size of 2.5 p*M* (1 p*M* = 10^{-12} moles/L). The concentrations are actually means along the approximately 600 m tow segments over which the syringes filled. Since the sampling sled was towed near the isopycnal surface of the release, these concentrations would have been near the maximum for their location. Concentrations above and below the sled would have decreased with vertical distance approximately in proportion to the average profile shown in Figure 12, the standard deviation of which is about 15 m. The most frequently encountered concentration was in the first histogram bin of 0–2.5 p*M*, since most of the area surveyed was devoid of tracer, and in fact the concentration in 105 of the 137 samples in that bin were zero. The histogram falls abruptly in the next four bins, to zero between 12.5 and 17.5 p*M*, with a few samples found in outlying bins between 17.5 and 27.5 p*M*. The largest concentration encountered was just slightly over 25 p*M*.

Histograms of the maximum concentration found at each station during the 4 and 12 month surveys are shown in Figures 16b and 16c, respectively. These concentrations are for spot samples captured with Niskin bottles, rather than averages along a tow track. Again, the maximum number of samples was in the first bin, and fell to zero after several bins, with a few concentrations in outlying bins. The maximum concentration at 4 months was 45 f*M* and at 12 months was 2.5 f*M*. With time, the peak in number in the first bin became less pronounced compared with the other bins, i.e., from initial to 4 to 12 month survey, as the tracer became more evenly distributed within the surveyed areas. These maximum concentrations were found near the target isopycnal surface. The distribution at other levels can be estimated from these histograms, but with the concentration scale diminished following the approximately Gaussian curves describing the mean vertical profiles, shown in Figures 12 and 14.

Because the vertical resolution of the SABGOM model is coarse compared with the narrow vertical width of the tracer distribution, it is best to compare column integrals rather than concentrations in the simulation with observations, as done in the maps of Figures 10 and 11. Figure 17 compares histograms of the observed column integrals at the stations of the 4 and 12 month surveys with histograms of simulated column integrals sampled at the same locations. The distributions of column integrals appear to be quite similar to one another. Perhaps the most important difference is that for the 12 month survey the first bin in the simulation is less populated than in the observations. That is, there are relatively fewer low concentrations

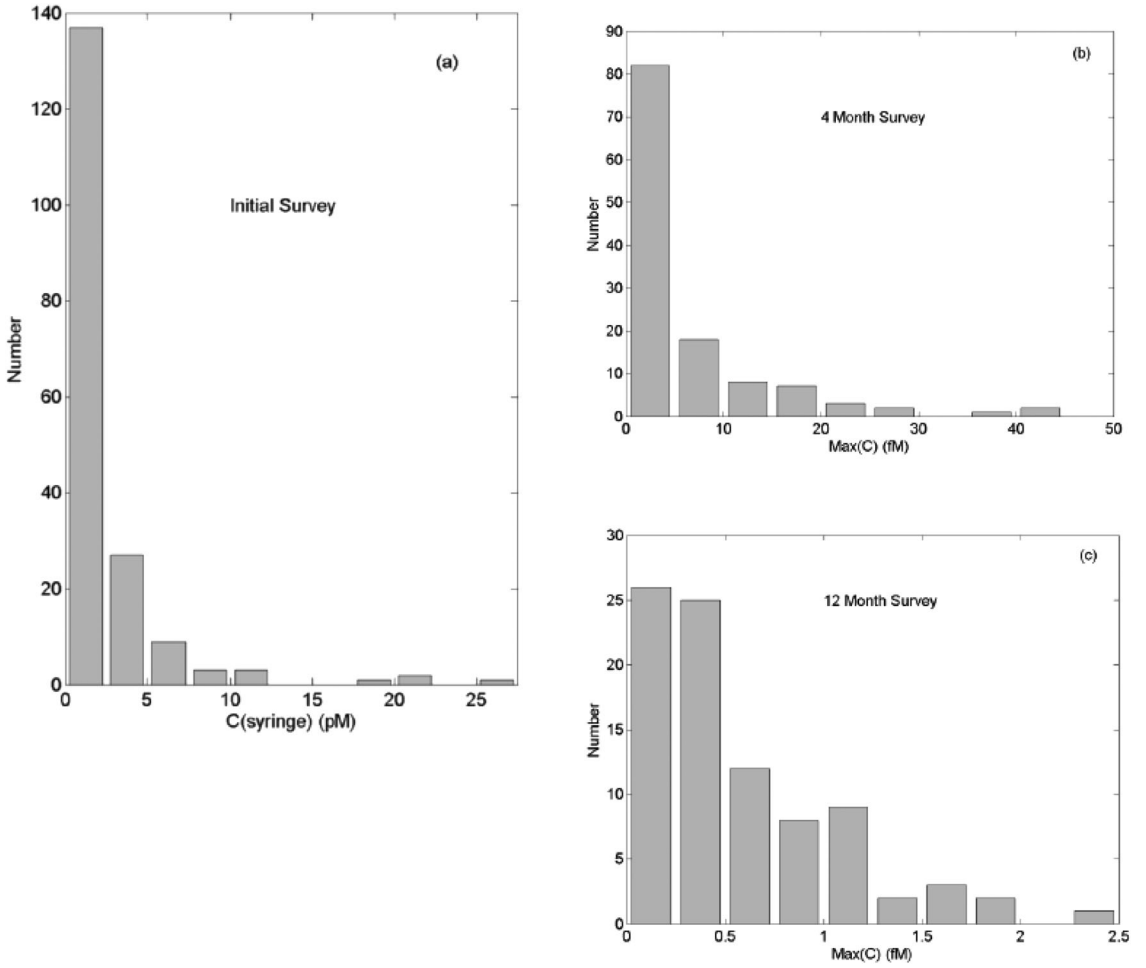

Figure 16. Histograms of maximum concentrations for the three surveys: (a) in the syringes in the system towed near the isopycnal surface of the release, in p*M*; (b, c) at the stations for the 4 and 12 month survey, respectively, in f*M*.

because the tracer is spread more homogeneously in the simulation than in the observations. This relative homogenization was suggested by the spatial autocorrelation.

5. Discussion

5.1. Boundary Mixing

In section 4, we showed that diapycnal dispersion of the tracer observed 4 months after the release was significantly greater for the profiles near the northern continental slope of the Gulf than in the interior. At 12 months, the diapycnal distribution of the tracer was not much changed from the mean interior distribution at 4 months, implying a diffusivity of 0.15×10^{-4} m^2/s, of order 10 times smaller than for the earlier period. We take these results as strong evidence that diapycnal mixing was greatly enhanced over the slope, since the tracer most likely spent more time over the slope during the first period than during the second period.

Time dependence, as well as this spatial dependence, is likely to have played a role, however. Hurricane Isaac passed directly over the site of the experiment about 1 month after the tracer release. The bottom-most moored current meters at the mooring sites indicated in Figure 4 show that more than 20% of the energy dissipation along the slope for the whole 12 month period probably occurred in the aftermath of this hurricane. Still, about as much energy was dissipated in the time interval between 4 and 12 months as during the first 4 months. By this measure, we would expect about the same amount of mixing in the two

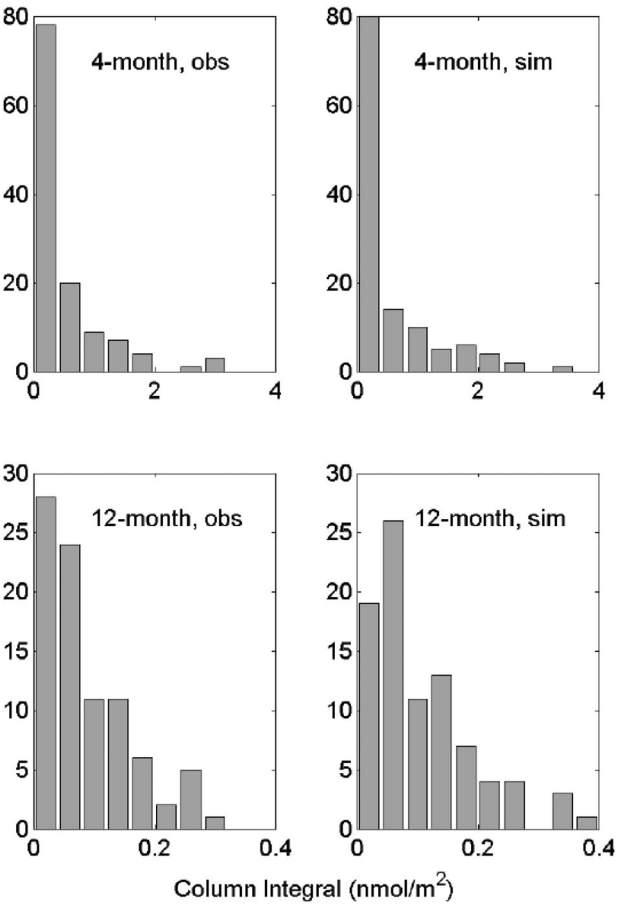

Figure 17. Histograms of the column integral observed (left) at the 4 and 12 month stations and (right) at those stations in the numerical simulation. The vertical axes give the number of stations in each bin. Note that the range of the horizontal axis is 10 times smaller at 12 months than at 4 months due to dispersion of the tracer.

periods if boundary mixing played a minor role, i.e., about the same increase in mean squared diapycnal dispersion of the tracer. Thus, the evidence for great enhancement near the boundaries is compelling.

We summarized many of the mechanisms forcing bottom currents along the slope in section 1. The dominant mechanism for our time period seems to be wind forcing, as discussed above, but Loop Current eddies and topographic Rossby waves propagating along the slope no doubt also played a role. Currents along the northern slope pass over a bottom that is corrugated with canyons and pimpled with salt domes (Figure 18). In work under way, K. Polzin and others speculate that form drag acting on flow over these features generates turbulent energy that is dissipated in a relatively shallow, but stratified, boundary layer, resulting in the strong mixing that we have observed.

The diapycnal diffusivity of 0.15×10^{-4} m^2/s, found for the *interior* between 4 and 12 months, is typical of open ocean conditions. For example, the value from the 30 month long tracer release experiment in the eastern subtropical gyre of the North Atlantic at 300–400 m depth was 0.17×10^{-4} m^2/s (LWL). The value found in the southeast Pacific sector of the Antarctic Circumpolar Current, a very energetic region, was 0.13×10^{-4} m^2/s near 1500 m depth [*Ledwell et al.*, 2011]. The diffusivity inferred from dissipation rates of turbulent kinetic energy at all depths, i.e., independent of buoyancy frequency, in the background internal wavefield at midlatitudes is even smaller, at approximately 0.05×10^{-4} m^2/s [*Gregg*, 1989; *Polzin et al.*, 1995]. Thus, conditions for turbulent mixing in the interior of the Gulf may be quite similar to those in the interior of the open ocean, far from topography.

5.2. Lateral Dispersion and Homogenization

Rates of lateral stirring and mixing and the consequent dilution of peak concentrations are of importance to the ecology of the middepth Gulf because of the potential for release of pollutants from drilling activities as well as the prevalence of natural hydrocarbon seeps. Lateral dispersion along isopycnal surfaces is far more effective at spreading and diluting a tracer than diapycnal dispersion, though the latter may play an important role in lateral dispersion through the process of shear dispersion at small scales. We estimate from the concentrations found that the area covered by the tracer at the time of the initial survey was about 50 km^2. After 1 year, the tracer was found spread over a good fraction of the Gulf, whose area at 1100 m is approximately 600,000 km^2. The peak concentration fell correspondingly, from 2.6×10^{-11} to 2.5×10^{-15} moles/kg. The mechanism for this huge dilution factor is stirring of the tracer by the shears and strains of boundary currents, mesoscale eddies, and a poorly understood cascade of smaller-scale motions, and then by the shear-induced turbulent events at submeter scales, and finally by molecular diffusion at scales of a centimeter or so.

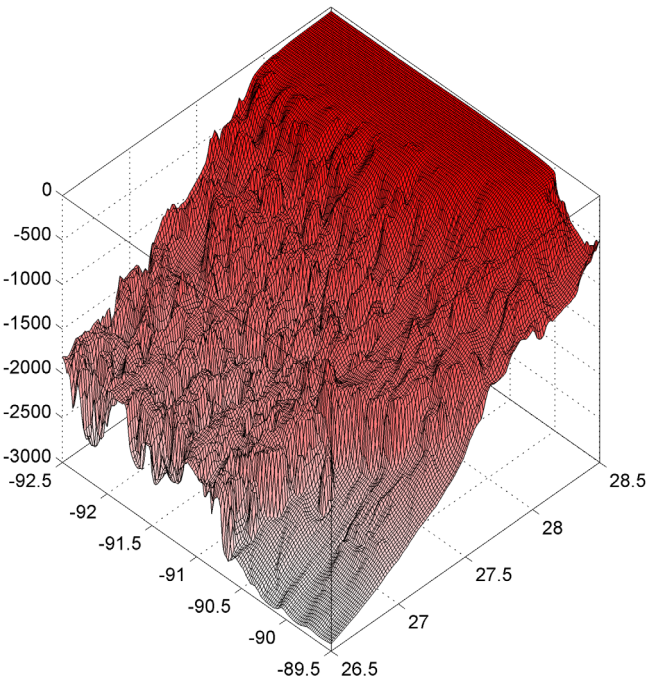

Figure 18. Example of the complex bathymetry of the continental slope along the northern Gulf of Mexico, from the region at which high tracer concentrations were found. Depth is in meters; the view is from the southeast. The map grid is 1.63 km × 1.83 km (zonal × meridional). Bathymetry data are from the NOAA National Geophysical Data Center, U.S. Coastal Relief Model, available at the web site http://www.ngdc.noaa.gov/mgg/coastal/crm.html.

Homogenization is a competition between stirring at small scales, tending to fill in the general area occupied by the tracer, against stirring at larger scales, tending to disperse the tracer and enlarge the overall area to be filled in [e.g., *Garrett*, 1983]. In the open ocean conditions of the North Atlantic Tracer Release Experiment (NATRE), tracer streaks 5 months after release were of order 10 km across, but separated by many tens of km, rendering the tracer very hard to find. One possible explanation for the relative homogeneity of the present tracer patch at 4 months is that it had been held close enough to the boundary for a long enough time to be spread into a broad band before it was carried away from the slope. It is also likely that shear dispersion associated with greatly enhanced diapycnal mixing over the slope helped broaden tracer streaks. Only after 12 months had the length scales of the spatial autocorrelation in the North Atlantic become as great as those in the present experiment at 4 months (compare Figures 15b and 15c).

An interesting question is the extent to which the tracer moved upward across the continental slope toward the shelf, shoreward of our stations. What evidence we have does not indicate such upwelling. Isopycnal surfaces consistently deepened toward the slope along the tow tracks shown in Figure 1. Downward dipping isopycnals are consistent with downwelling bottom Ekman currents resulting from southwestward flow along the slope. Also, our boundary stations during the surveys at 4 and 12 months are generally within 30 km of the grounding lines of the isopycnal surfaces occupied by the tracer. We estimate from our results on lateral dispersion that the time for communication between these grounding lines and the stations is a month or two, so that the boundary profiles seen in Figures 7 and 9 and the mean boundary profile in Figure 12 may well be representative of what tracer has made it up the slope.

5.3. Peak Concentrations

The maximum of all the concentrations found during each survey is shown in Figure 19. The concentration in the initial plume of the injection sled is estimated to have been about 9×10^{-7} moles/kg (the first point shown in Figure 19). The maximum concentrations actually observed during the three surveys are shown as the last three points lying on a straight line in Figure 19. These suggest a $t^{-2.5}$ dependence, where t is the time since release.

This last result is reminiscent of the diffusion diagrams of *Okubo* [1971], who found that the area of dye patches released in the upper ocean in coastal and shelf areas grew like $t^{2.34}$. Aside from the fact that vertical mixing in the present experiment would add another 0.5 to the exponent, this apparent agreement conceals several aspects of dispersion in the present experiment that are absent in the experiments synthesized by Okubo. First of all, there may be enhanced dispersion near the slope due to cross-slope shear in the along-slope currents coupled with cross-slope diffusivity. Then, as part of the patch leaves the boundary region, it would be stirred by eddies into filaments with an exponential growth in the along-filament direction, and perhaps a cross filament scale that is not growing at all or is even shrinking because

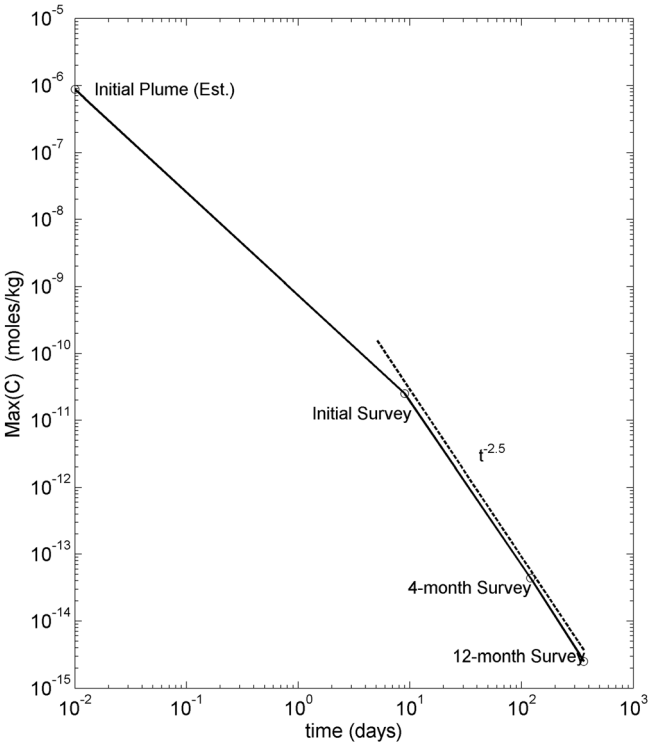

Figure 19. Maximum tracer concentration as a function of time. The point labeled "Initial Plume (Est.)" is an estimate for the tracer concentration in the initial turbulent plume of the injection sled. The dashed line along the survey points indicates a $t^{-2.5}$ power law.

of convergence in the cross-filament direction [e.g., *Garrett*, 1983]. Thus, several processes, some no doubt not mentioned here, go into the trend in Figure 19. Nevertheless, the order of magnitude of the dilution over the various time scales of the experiment, i.e., 10 days or so for the initial survey, and then 4 and 12 months for the subsequent surveys, provide useful phenomenology for dispersion near the continental slope and interior of the Gulf: we see a time dependence of the maximum concentration of $t^{-2.5}$ for time t between 10 days and 12 months after the release.

A power law dependence of peak concentration stronger than -1.5 implies that lateral dispersion was "superdiffusive," that is exhibiting a stronger time dependence than Fickian diffusion. Super diffusive dispersion of surface drifters was also found by *LaCasce and Ohlmann* [2003] for the surface waters of the northern shelf and slope of the Gulf, though they were able to discern periods of exponential growth and power law growth from their detailed time series of many pairs and triplets of drifters. Our study is of stirring at 1100 m, where kinetic energy is much lower than near the surface, and Eulerian time scales appear to be rather different [see, e.g., *Hamilton*, 1990; *Hamilton and Lugo-Fernandez*, 2001]. Nevertheless, superdiffusive dispersion seems to be more the norm than the exception in the Gulf at least at scales below the mesoscale.

6. Summary

The following conclusions may be drawn from the experiment:

1. Diapycnal mixing at middepth in the northern Gulf of Mexico is much greater near the continental slope than in the interior, where it is approximately 0.15×10^{-4} m^2/s, a value typical of the open ocean.
2. Homogenization of a tracer released near the slope proceeds faster than in the open ocean; fast enough to sample effectively with discrete stations after a few months.
3. Concentrations of a tracer released along the slope at middepth fell by a factor of approximately 200 in a period of 10 days or so, by a factor of 10^5 over 4 months, and by another factor of 10 over the next 8 months.

Understanding the physics behind these conclusions will benefit from past work, and especially from measurements made concurrently with the tracer experiment by the GISR mooring array, and from fine and microstructure profiles made as part of GISR. Analysis and interpretation of these data are under way. The SABGOM numerical simulation was able to replicate important statistics of observed tracer and helped interpret the dispersion of the tracer, and especially the evolution of streakiness and of the concentration distribution. Conversely, the behavior of the tracer and its explanation in terms of forcing will help to develop more advanced numerical schemes and next generation ocean models that could be used to better forecast the trajectories, concentrations, and the fate of substances released at depth in the Gulf of Mexico, either accidentally or naturally.

Acknowledgments

The skill and cooperation of the masters and crew of R/V *Brooks McCall*, operated by TDI Brooks, Inc., and of R/V *Pelican*, operated by the Louisiana Universities Marine Consortium (LUMCON), were essential to the success of the cruises. Jim Brooks and Leslie Bender of TDI Brooks and Joe Malbrough of LUMCON, and their staffs were of great help with preparations and contractual arrangements. Invaluable assistance in the field was rendered by Stew Sutherland of LDEO, by Brian Guest, Leah Houghton, Ann Lovely, Cynthia Sellers, Alexi Shalapyonok, all of WHOI, Eric Quiroz of TAMU, Angel Ruiz Angulo of UNAM, Diego Lopez Veneroni of IMP, and by students Hannah Baker, Reagan Errera, Laure Harred, Ivan Maulana, Noura Randle, Charlene Ren, Allison Smyth, Jordan Young, and Luz Zarote. The mooring system used to track the RAFOS floats was deployed by Amy Bower at WHOI, as part of a study funded by the Bureau of Ocean Energy Management, Regulation and Enforcement. RAFOS floats were prepared with the help of Jim Valdes at WHOI. Tracks were analyzed by Heather Furey at WHOI. R. Leben and M. Shannon at the Colorado Center for Astrodynamics Research responded with alacrity on a weekend with help with altimetry maps. The work described here is part of the Gulf Integrated Spill Response Consortium (GISR), whose lead institution is TAMU. We thank Scott Socolofsky, co-PI of GISR with P. Chapman, administrator Laura Caldwell, and staff at TAMU, as well as Linda Cannata and staff at WHOI, for their work on contractual arrangements, and Marjorie Parmenter for help preparing the manuscript. This research was made possible by a grant from The Gulf of Mexico Research Initiative. Data are publicly available through the Gulf of Mexico Research Initiative Information & Data Cooperative (GRIIDC) at https://data.gulfresearchinitiative.org (doi:10.7266/N79P2ZK2, doi:10.7266/N75X26VQ, and doi:10.7266/N7251G4Q).

References

Badan, A., J. Candela, J. Sheinbaum, and J. Ochoa (2005), Upper-layer circulation in the approaches to Yucatan Channel, in *Circulation in the Gulf of Mexico: Observations and Models, Geophys. Monogr. Ser.*, vol. 161, edited by W. Sturges III and A. Lugo-Fernandez, pp. 57–69, AGU, Washington, D. C.

Banyte, D., T. Tanhua, M. Visbeck, D. W. R. Wallace, J. Karstensen, G. Krahmann, A. Schneider, L. Stramma, and M. Dengler (2012), Diapycnal diffusivity at the upper boundary of the tropical North Atlantic oxygen minimum zone, *J. Geophys. Res.*, *117*, C09016, doi:10.1029/2011JC007762.

Boland, E. J. D., E. Shuckburgh, P. H. Haynes, J. R. Ledwell, M.-J. Messias, and A. J. Watson (2015), Determining a sub-mesoscale diffusivity using a roughness measure applied to a tracer release experiment in the Southern Ocean, *J. Phys. Oceanogr.*, *45*, 1610–1631, doi:10.1175/JPO-D-14-0047.1.

Bretherton, F. P., R. E. Davis, and C. B. Fandry (1976), A technique for objective analysis and design of oceanographic experiments applied to MODE-73, *Deep Sea Res. Oceanogr. Abstr.*, *23*(7), 559–582, doi:10.1016/0011-7471(76)90001-2.

Bunge, L., J. Ochoa, A. Badan, J. Candela, and J. Sheinbaum (2002), Deep flows in the Yucatan Channel and their relation to changes in the Loop Current extension, *J. Geophys. Res.*, *107*(C12), 3233, doi:10.1029/2001JC001256.

Camilli, R., C. M. Reddy, D. R. Yoerger, B. A. S. Van Mooy, M. V. Jakuba, J. Kinsey, C. P. McIntyre, S. P. Sylva, and J. V. Maloney (2010), Tracking hydrocarbon plume transport and biodegradation at Deepwater Horizon, *Science*, *330*, 201–204, doi:10.1126/science.1195223.

Candela, J., J. Sheinbaum, J. Ochoa, and A. Badan (2002), The potential vorticity flux through the Yucatan Channel and the Loop Current in the Gulf of Mexico, *Geophys. Res. Lett.*, *29*(22), 2059, doi:10.1029/2002GL015587.

Chassignet, E. P., H. E. Hurlburt, O. M. Smedstad, G. R. Halliwell, P. J. Hogan, A. J. Wallcraft, R. Baraille, and R. Bleck (2007), The HYCOM (hybrid coordinate ocean model) data assimilative system, *J. Mar. Syst.*, *65*, 60–83.

Chassignet, E. P., et al. (2009), U.S. GODAE: Global ocean prediction with the hybrid coordinate ocean model (HYCOM), *Oceanography*, *22*(3), 48–59.

Cherubin, L. M., W. Sturges, and E. P. Chassignet (2005), Deep flow variability in the vicinity of the Yucatan Straits from a high-resolution numerical simulation, *J. Geophys. Res.*, *110*, C04009, doi:10.1029/2004JC002280.

Egbert, G. D., and S. Y. Erofeeva (2002), Efficient inverse modeling of barotropic ocean tides, *J. Atmos. Oceanic Technol.*, *19*, 183–204, doi:10.1175/1520-0426(2002)019 < 0183:EIMOBO > 2.0.CO;2.

Effron, B., and G. Gong (1983), A leisurely look at the bootstrap, the jackknife, and cross-validation, *Am. Stat.*, *37*, 36–48.

Garrett, C. (1983), On the initial streakiness of a dispersing tracer in two- and three-dimensional turbulence, *Dyn. Atmos. Oceans*, *7*(4), 265–277, doi:10.1016/0377-0265(83)90008-8.

Gregg, M. C. (1989), Scaling turbulent dissipation in the thermocline, *J. Geophys. Res.*, *94*(C7), 9689–9698.

Haidvogel, D. B., and T. Keffer (1984), Tracer dispersal by mid-ocean mesoscale eddies, Part I. Ensemble statistics, *Dyn. Atmos. Oceans*, *8*(1), 1–40, doi:10.1016/0377-0265(84)90002-2.

Haidvogel, D. B., et al. (2008), Ocean forecasting in terrain-following coordinates: Formulation and skill assessment of the regional ocean modeling system, *J. Comput. Phys.*, *227*, 3595–3624.

Halliwell, G. R., Jr., A. Srinivasan, V. Kourafalou, H. Yang, D. Willey, M. Le Henaff, and R. Atlas (2014), Rigorous evaluation of a fraternal twin ocean OSSE system in the open Gulf of Mexico, *J. Atmos. Oceanic Technol.*, *31*, 105–130, doi:10.1175/JTECH-D-13-00011.1.

Hamilton, P. (1990), Deep currents in the Gulf of Mexico, *J. Phys. Oceanogr.*, *20*(7), 1087–1104, doi:10.1175/1520-0485(1990)020<1087:DCITGO>2.0.CO;2.

Hamilton, P. (2009), Topographic Rossby waves in the Gulf of Mexico, *Prog. Oceanogr.*, *82*(1), 1–31, doi:10.1016/j.pocean.2009.04.019.

Hamilton, P., and T. N. Lee (2005), Eddies and jets over the slope of the northeast Gulf of Mexico, in *Circulation in the Gulf of Mexico: Observations and Models, Geophys. Monogr. Ser.*, vol. 161, edited by W. Sturges III and A. Lugo-Fernandez, pp. 123–142, AGU, Washington, D. C.

Hamilton, P., and A. Lugo-Fernandez (2001), Observations of high speed deep currents in the northern Gulf of Mexico, *Geophys. Res. Lett.*, *28*(14), 2867–2870, doi:10.1029/2001GL013039.

He, R., and R. H. Weisberg (2002), Tides on the West Florida Shelf, *J. Phys. Oceanogr.*, *32*(12), 3455–3473.

Ho, D. T., J. R. Ledwell, and W. M. Smethie Jr. (2008), Use of SF_5CF_3 for ocean tracer release experiments, *Geophys. Res. Lett.*, *35*, L04602, doi:10.1029/2007GL032799.

Holtermann, P. L., L. Umlauf, T. Tanhua, O. Schmale, G. Rehder, and J. Waniek (2012), The Baltic Sea tracer release experiment: 1. Mixing rates, *J. Geophys. Res.*, *117*, C01021, doi:10.1029/2011/JC007439.

Hurlburt, H. E., and J. D. Thompson (1980), A numerical study of Loop Current intrusions and eddy shedding, *J. Phys. Oceanogr.*, *10*, 1611–1651.

Hyun, H. H., and R. He (2010), Coastal upwelling in the South Atlantic Bight: A revisit of the 2003 cold event using long term observations and model hindcast solutions, *J. Mar. Syst.*, *83*, 1–13, doi:10.1016/j.jmarsys.2010.05.014.

Jaimes, B., and L. K. Shay (2010), Near-inertial wave wake of hurricanes Katrina and Rita over mesoscale oceanic eddies, *J. Phys. Oceanogr.*, *40*, 1320–1337.

Journel, A. G., and Ch. J. Huijbregts (1978), *Mining Geostatistics*, 600 pp., Academic, San Diego, Calif.

Kantha, L. (2005), Barotropic tides in the Gulf of Mexico, in *Circulation in the Gulf of Mexico: Observations and Models, Geophys. Monogr. Ser.*, vol. 161, edited by W. Sturges and A. Lugo-Fernandez, pp. 159–163, AGU, Washington, D. C.

LaCasce, J. H., and C. Ohlmann (2003), Relative dispersion at the surface of the Gulf of Mexico, *J. Mar. Res.*, *61*, 285–312.

Law, C. S., A. J. Watson, and M. I. Liddicoat (1994), Automated vacuum analysis of sulphur hexafluoride in seawater: Derivation of the atmospheric trend (1970-1993) and potential as a transient tracer, *Mar. Chem.*, *48*, 57–60, doi:10.1016/0304-4203(94)90062-0.

Leben, R. R. (2005), Altimeter-derived Loop Current metrics, in *Circulation in the Gulf of Mexico: Observations and Models, Geophys. Monogr. Ser.*, vol. 161, edited by W. Sturges III and A. Lugo-Fernandez, pp. 181–201, AGU, Washington, D. C.

Ledwell, J. R., and A. Bratkovich (1995), A tracer study of mixing in the Santa Cruz Basin, *J. Geophys. Res.*, *100*(C10), 20,681–20,704, doi:10.1029/95JC02164.

Ledwell, J. R., and B. M. Hickey (1995), Evidence for enhanced boundary mixing in the Santa Monica Basin, *J. Geophys. Res.*, *100*(C10), 20,665–20,679, doi:10.1029/94JC01182.

Ledwell, J. R., A. J. Watson, and C. S. Law (1993), Evidence for slow mixing across the pycnocline from an open-ocean tracer-release experiment, *Nature*, *364*(6439), 701–703, doi:10.1038/364701a0.

Ledwell, J. R., A. J. Watson, and C. S. Law (1998), Mixing of a tracer in the pycnocline, *J. Geophys. Res.*, *103*(C10), 21,499–21,529, doi:10.1029/98JC01738.

Ledwell, J. R., E. T. Montgomery, K. L. Polzin, L. C. St. Laurent, R. W. Schmitt, and J. M. Toole (2000), Evidence for enhanced mixing over rough topography in the abyssal ocean, *Nature*, *403*(6766), 179–182, doi:10.1038/35003164.

Ledwell, J. R., L. C. St. Laurent, J. B. Girton, and J. M. Toole (2011), Diapycnal mixing in the Antarctic Circumpolar Current, *J. Phys. Oceanogr.*, *41*(1), 241–246, doi:10.1175/2010JPO4557.1.

Lee, M.-M., A. J. G. Nurser, A. C. Coward, and B. A. De Cuevas (2009), Effective eddy diffusivities inferred from a point release tracer in an eddy-resolving model, *J. Phys. Oceanogr.*, *39*, 894–914, doi:10.1175/2008JPO3902.1.

Lubchenco, J., M. K. McNutt, G. Dreyfus, S. A. Murawski, D. M. Kennedy, P. T. Anastas, S. Chu, and T. Hunter (2012), Science in support of the Deepwater Horizon response, *Proc. Natl. Acad. Sci. U. S. A.*, *109*(50), 20,212–21,221, doi:10.1073/pnas.1204729109.

Marchesiello, P., L. Debreu, and X. Couvelard (2009), Spurious diapycnal mixing in terrain-following coordinate models: The problem and a solution, *Ocean Modell.*, *26*, 156–169.

Mellor, G. L., and T. Yamada (1982), Development of a turbulence closure model for geophysical fluid problems, *Rev. Geophys.*, *20*(4), 851–875.

Morey, S. L., J. Zavala-Hidalgo, and J. J. O'Brien (2005), The seasonal variability of continental shelf circulation in the northern and western Gulf of Mexico from a high-resolution numerical model, in *Circulation of the Gulf of Mexico: Observations and Models, Geophys. Monogr. Ser.*, vol. 161, edited by W. Sturges and A. Lugo-Fernandez, AGU, Washington, D. C.

North, E., E. Adams, A. Thessen, Z. Schlag, R. He, S. Socolofsky, S. Masutani, and S. Peckham (2015), The influence of droplet size and biodegradation on the transport of subsurface oil droplets during the Deepwater Horizon spill: A model sensitivity study, *Environ. Res. Lett.*, *10*, 024016, doi:10.1088/1748-9326/10/2/024016.

North, E. W., E. Adams, Z. Schlag, C. R. Sherwood, R. He, K. H. Hyun, and S. A. Socolofsky (2011), Simulating oil droplet dispersal from the Deepwater Horizon spill with a Lagrangian approach, in *Monitoring and Modeling the Deepwater Horizon Oil Spill: A Record-Breaking Enterprise, Geophys. Monogr. Ser.*, vol. 195, edited by Y. Liu et al., pp. 217–226, AGU, Washington, D. C.

Ochoa, J., J. Sheinbaum, A. Badan, J. Candela, and D. Wilson (2001), Geostrophy versus potential vorticity inversion in the Yucatan Channel, *J. Mar. Res.*, *59*, 725–747.

Oey, L.-Y. (1996), Simulation of mesoscale variability in the Gulf of Mexico: Sensitivity studies, comparison with observations, and trapped wave propagation, *J. Phys. Oceanogr.*, *26*, 145–175.

Oey, L.-Y., and H.-C. Lee (2002), Deep eddy energy and topographic Rossby waves in the Gulf of Mexico, *J. Phys. Oceanogr.*, *32*(12), 3499–3527, doi:10.1175/1520-0485(2002)032 < 3499:DEEATR>2.0.CO;2.

Oey, L.-Y., M. Inoue, R. Lai, X.-H. Xin, S. E. Welsh, and L. J. Rouse (2008), Stalling of near-inertial waves in a cyclone, *Geophys. Res. Lett.*, *35*, L12604, doi:10.1029/2008GL034273.

Okubo, A. (1971), Oceanic diffusion diagrams, *Deep Sea Res. Oceanogr. Abstr.*, *18*(8), 789–802, doi:10.1016/0011-7471(71)90046-5.

Poje, A. C., et al. (2014), Submesoscale dispersion in the vicinity of the Deepwater Horizon spill, *Proc. Natl. Acad. Sci. U. S. A.*, *111*, 12,693–12,698, doi:10.1073/pnas.1402452111.

Polzin, K., and R. Ferrari (2004), Isopycnal dispersion in NATRE, *J. Phys. Oceanogr.*, *34*(1), 247–257, doi:10.1175/1520-0485(2004)034 < 0247:IDIN>2.0.CO;2.

Polzin, K., J. M. Toole, and R. W. Schmitt (1995), Finescale parameterizations of turbulent dissipation, *J. Phys. Oceanogr.*, *25*(3), 306–328, doi:10.1175/1520-0485(1995)025 < 0306:FPOTD>2.0.CO;2.

Polzin, K. L., J. M. Toole, J. R. Ledwell, and R. W. Schmitt (1997), Spatial variability of turbulent mixing in the abyssal ocean, *Science*, *276*(5309), 93–96, doi:10.1126/science.276.5309.93.

Rivas, D., A. Badan, and J. Ochoa (2005), The ventilation of the deep Gulf of Mexico, *J. Phys. Oceanogr.*, *35*, 1763–1781.

Schmitz, W. J., Jr. (2005), Cyclones and westward propagation in the shedding of anticyclonic rings from the Loop Current, in *Circulation in the Gulf of Mexico: Observations and Models, Geophys. Monogr. Ser.*, vol. 161, edited by W. Sturges III and A. Lugo-Fernandez, pp. 241–261, AGU, Washington, D. C.

Schmitz, W. J., Jr., D. C. Biggs, A. Lugo-Fernandez, L.-Y. Oey, and W. Sturges (2005), A synopsis of the circulation in the Gulf of Mexico and on its continental margins, in *Circulation in the Gulf of Mexico: Observations and Models, Geophys. Monogr. Ser.*, vol. 161, edited by W. Sturges III and A. Lugo-Fernandez, pp. 11–29, AGU, Washington, D. C.

Shay, L. K., A. J. Mariano, S. D. Jacob, and E. H. Ryan (1998), Mean and near-inertial ocean current response to Hurricane Gilbert, *J. Phys. Oceanogr.*, *28*, 858–889.

Shchepetkin, A. F., and J. C. McWilliams (2005), The regional ocean modeling system (ROMS): A split-explicit, free-surface, topography-following coordinates ocean model, *Ocean Modell.*, *9*, 347–404.

Sheinbaum, J., J. Candela, A. Badan, and J. Ochoa (2002), Flow structure and transport in the Yucatan Channel, *Geophys. Res. Lett.*, *29*(3), 1040, doi:10.1029/2001GL013990.

Smith, K. S., and R. Ferrari (2009), The production and dissipation of compensated thermohaline variance by mesoscale stirring, *J. Phys. Oceanogr.*, *39*, 2477–2501, doi:10.1175/2009JPO4103.1.

Smolarkiewicz, P. K. (1984), A fully multidimensional positive definite advection transport algorithm with small implicit diffusion, *J. Comput. Phys.*, *54*, 325–362.

Sturges, W. (2005), Deep-water exchange between the Atlantic, Caribbean, and Gulf of Mexico, in *Circulation in the Gulf of Mexico: Observations and Models, Geophys. Monogr. Ser.*, vol. 161, edited by W. Sturges III and A. Lugo-Fernandez, pp. 263–278, AGU, Washington, D. C.

Sturges, W., and R. Leben (2000), Frequency of ring separations from the loop current in the Gulf of Mexico: A revised estimate, *J. Phys. Oceanogr.*, *30*, 1814–1819.

Sturges, W., III, and A. Lugo-Fernandez (2005), *Circulation in the Gulf of Mexico: Observations and Models, Geophys. Monogr. Ser.*, vol. 161, AGU, Washington, D. C.

Sturges, W. T., et al. (2000), A potent greenhouse gas identified in the atmosphere: SF_5CF_3, *Science*, *289*, 611–613.

Sundermeyer, M. A., and J. F. Price (1998), Lateral mixing and the North Atlantic tracer release experiment: Observations and numerical simulations of Lagrangian particles and passive tracer, *J. Geophys. Res.*, *103*(C10), 21,481–21,497, doi:10.1029/98JC01999.

Sundermeyer, M. A., J. R. Ledwell, N. S. Oakey, and B. J. W. Greenan (2005), Stirring by small-scale vortices caused by patchy mixing, *J. Phys. Oceanogr.*, *35*(7), 1245–1262, doi:10.1175/JPO2713.1.

Tulloch, R., R. Ferrari, O. Jahn, A. Klocker, J. LaCasce, J. R. Ledwell, J. Marshall, M.-J. Messias, K. Speer, and A. J. Watson (2014), Direct estimate of lateral eddy diffusivity upstream of Drake Passage, *J. Phys. Oceanogr.*, *44*, 2593–2616, doi:10.1175/JPO-D-13-0120.1.

Wanninkhof, R., J. R. Ledwell, and A. J. Watson (1991), Analysis of sulfur hexafluoride in seawater, *J. Geophys. Res.*, *96*(C5), 8733–8740, doi:10.1029/91JC00104.

Watson, A. J., J. R. Ledwell, M.-J. Messias, B. A. King, N. Mackay, M. P. Meredith, B. Mills, and A. C. Naveira Garabato (2013), Rapid cross-density ocean mixing at mid depths in Drake Passage, *Nature*, *501*, 408–411, doi:10.1038/nature12432.

Weisberg, R. H., L. Zheng, and Y. Liu (2011), Tracking subsurface oil in the aftermath of the Deepwater Horizon well blowout, in *Monitoring and Modeling the Deepwater Horizon Oil Spill: A Record-Breaking Enterprise, Geophys. Monogr. Ser.*, vol. 195, edited by Y. Liu et al., pp. 205–215, AGU, Washington, D. C.

Xue, Z., R. He, K. Fennel, W.-J. Cai, S. Lohrenz, and C. Hopkinson (2013), Modeling ocean circulation and biogeochemical variability in the Gulf of Mexico, *Biogeosci.*, *10*, 7219–7234, doi:10.5194/bg-10-7219-2013.

Xue, Z., J. Zambon, Z. Yao, Y. Liu, and R. He (2015), An integrated ocean circulation, wave, atmosphere, and marine ecosystem prediction system for the South Atlantic Bight and Gulf of Mexico, *J. Operational Oceanogr.*, *8*, 80–91, doi:10.1080/1755876X.2015.1014667.